

Journal of Cerebral Blood Flow & Metabolism

Official Journal of the International Society of Cerebral Blood Flow and Metabolism

EDITOR-IN-CHIEF

James McCulloch

*Wellcome Surgical Institute & Hugh Fraser Neuroscience Labs.,
University of Glasgow, Garscube Estate, Bearsden Road,
Glasgow G61 1QH, Scotland, U.K.
Telephone: (+44)-141-330-6981
Fax: (+44)-141-943-0215
e-mail: ljt2h@udcf.gla.ac.uk*

DEPUTY CHIEF EDITORS

U. Dirnagl, Berlin **S.-C. Huang, Los Angeles**
R. S. J. Frackowiak, London **T. Kirino, Tokyo**

ASSOCIATE EDITORS

D. Dewar, Glasgow **I. M. Macrae, Glasgow**

HONORARY EDITOR

Seymour S. Kety, Bethesda

EDITORIAL BOARD

K. Abe, Sendai	J. H. Greenberg, Philadelphia	M. A. Moskowitz, Boston
R. N. Auer, Calgary	A. Grinvald, Rehovot	M. Nedergaard, Valhalla
J.-C. Baron, Caen	J. M. Hallenbeck, Bethesda	T. S. Nowak, Jr., Memphis
R. Bullock, Richmond	K. Herholz, Cologne	W. D. Obrist, Pittsburgh
R. E. Carson, Bethesda	P. Herscovitch, Bethesda	E. Pinard, Paris
P. H. Chan, San Francisco	C. Y. Hsu, St. Louis	N. J. Rothwell, Manchester
M. Chopp, Detroit	C. Iadecola, Minneapolis	K. C. Schmidt, Bethesda
F. M. Faraci, Iowa City	M. Ingvar, Stockholm	A. Schousboe, Copenhagen
G. Z. Feuerstein, King of Prussia	I. Kanno, Akita	G. K. Steinberg, Stanford
K. A. Frey, Ann Arbor	M. Kiessling, Heidelberg	R. J. Traystman, Baltimore
Y. Fukuchi, Tokyo	J. Kriegstein, Marburg	S. J. Warach, Boston
A. H. Gjedde, Aarhus	W. D. Lust, Cleveland	S. G. Waxman, New Haven
	M. Moseley, Stanford	

PUBLICATION COMMITTEE

L. Sokoloff, Bethesda (Chair)	F. Gotoh, Tokyo
J. McCulloch, Glasgow (ex-officio)	R. J. Traystman, Baltimore
J. M. Hallenbeck, Bethesda	W.-D. Heiss, Cologne
R. S. J. Frackowiak, London	

EMERITUS EDITORS

A. M. Harper, 1981-1988
K.-A. Hossmann, 1989-1992
M. D. Ginsberg, 1992-1997

PUBLICATION STAFF

Lindsey J. Towers
Assistant to the Editor-in-Chief
Glasgow

Nancy Megley
Publisher
Lippincott Williams & Wilkins

Denise Martin
Production Editor
Lippincott Williams & Wilkins

Ray Thibodeau
Director, Advertising Sales
Lippincott Williams & Wilkins

Qun Wang
Manufacturing Coordinator
Lippincott Williams & Wilkins

An Adiabatic Approximation to the Tissue Homogeneity Model for Water Exchange in the Brain: I. Theoretical Derivation

Keith S. St. Lawrence and Ting-Yim Lee

Department of Diagnostic Radiology and the Lawson Research Institute, St. Joseph's Health Centre, and the Imaging Research Laboratories, Robarts Research Institute, London, Ontario, Canada

Summary: Using the adiabatic approximation, which assumes that the tracer concentration in parenchymal tissue changes slowly relative to that in capillaries, we derived a time-domain, closed-form solution of the tissue homogeneity model. This solution, which is called the adiabatic solution, is similar in form to those of two-compartment models. Owing to its simplicity, the adiabatic solution can be used in CBF experiments in which kinetic data with only limited time resolution or signal-to-noise ratio, or both, are obtained. Using computer simulations, we investigated the accuracy and the precision of the parameters in the adiabatic solution for values that reflect ^2H -labeled water (D_2O) clearance from the brain (see Part II). It

was determined that of the three model parameters, (1) the vascular volume (V_v), (2) the product of extraction fraction and blood flow (EF), and (3) the clearance rate constant (k_{ex}), only the last one could be determined accurately, and therefore CBF must be determined from this parameter only. From the error analysis of the adiabatic solution, it was concluded that for the D_2O clearance experiments described in Part II, the coefficient of variation of CBF was approximately 7% in gray matter and 22% in white matter. **Key Words:** Cerebral blood flow—Tracer kinetics—Deuterium oxide—Nuclear magnetic resonance—Compartmental modeling.

Because of the reliance of the brain on blood flow to deliver oxygen and nutrients continuously to meet its metabolic demands, there has been a great deal of interest in measuring CBF in both research and clinical practice. One popular method, which was proposed more than 40 years ago, is to monitor the passage of a diffusible tracer through brain tissue (Kety, 1951). A diffusible tracer is any substance whose exchange between blood and tissue is mediated by diffusion. Water is one such substance and water labeled with radioactive oxygen (H_2^{15}O) has been used extensively as a tracer with pos-

itron emission tomography since the 1980s (Frackowiak et al., 1980; Huang et al., 1982; Raichle et al., 1983). With the development of nuclear magnetic resonance for *in vivo* studies, techniques using nuclear magnetic resonance and water labeled with either ^2H , ^{17}O , or spin tagging have subsequently been developed (Corbett et al., 1991; Detre et al., 1990; Kim and Ackerman, 1990; Pekar et al., 1991; Williams et al., 1992).

A concern with the use of labeled water has been the observation that the CBF estimate is dependent on the experimental duration (Ginsberg et al., 1982; Raichle et al., 1983). This dependency manifests itself as a decrease in the CBF estimate with increasing experimental time and has been referred to as the falling flow phenomenon (FFP). Larson et al. (1987) concluded that the FFP is a result of the inadequacies of the single-compartment model, as proposed by Kety (1951), in describing the exchange of water between blood and parenchymal tissue in the brain. They proposed a two-barrier distributed-parameter model to replace the Kety model. However, the two-barrier model has seen limited usage because of its mathematical complexity (Quarles et al., 1993). The objective of this investigation is to develop a model that is mathematically simpler than the two-barrier model, yet realistic enough to eliminate the FFP.

Received February 24, 1997; final revision received January 6, 1998; accepted April 2, 1998.

This project was supported by the Medical Research Council of Canada, the National Cancer Institute of Canada, the Ontario Heart and Stroke Foundation, the Sterling-Windrop Imaging Research Institute, and the University Research Incentive Fund, Ontario Ministry of Colleges and Universities. Keith S. St. Lawrence was supported by a Medical Research Council of Canada Studentship and the Academic Development Fund of the London X-ray Associates.

Address correspondence and reprint requests to T.-Y. Lee, PhD, FCCPM, Department of Radiology, St. Joseph's Health Centre, 268 Grosvenor Street, London Ontario, Canada N6A 4V2.

Abbreviations used: COV, covariance matrix; CV, coefficient of variance; D_2O , ^2H -labeled water; EF , product of extraction fraction and blood flow; EVS, extravascular space; FFP, falling flow phenomenon; IVS, intravascular space; k_{ex} , clearance rate constant; SNR, signal-to-noise ratio; TH, tissue homogeneity; V_v , vascular volume.

When choosing the appropriate tracer kinetics model, there is always a compromise between mathematical complexity, which is dictated by the number of exchange processes modeled, and the practical limits set by the data (i.e., temporal resolution and signal-to-noise ratio, SNR). One of the more simple among distributed parameter models is the tissue homogeneity (TH) model, which was initially developed by Johnson and Wilson (1966) and subsequently proposed for tracer transport in the brain by Sawada et al. (1989). This model differs from the two-barrier model in that it has only one diffusion barrier separating the capillary space from the parenchymal tissue space. In addition, whereas the tracer concentration in the capillary space depends on spatial variables and time, that in the parenchymal tissue space is just dependent on time alone, i.e., it is assumed to be a compartment. In this paper, we will demonstrate that a closed-form solution in the time domain to the mass balance equations defined by the TH model can be derived using the adiabatic approximation. This approximation, which is discussed in the next section, is based on the difference in the rate of change of the tracer concentration in the capillary (intravascular) space compared with that in the parenchymal tissue (extravascular) space. The simplified time-domain solution, which we call the adiabatic solution, is the sum of two terms: one represents the transit of the tracer through the intravascular space and the other represents the clearance of the extracted fraction of tracer from the extravascular space.

Along with the derivation of the adiabatic solution, the results of computer simulations demonstrating the validity of the adiabatic approximation are presented in this paper. As well, the precision of the model parameters in the adiabatic solution was investigated using statistical error analysis. This analysis was conducted for parameter values that reflect the range of values observed in CBF experiments. In the accompanying paper, CBF measurements obtained using the tracer D_2O and the proposed adiabatic solution will be presented.

THEORY

Kety model

For reference, we begin with a brief description of the Kety model (Kety, 1951), which has been employed extensively in tracer kinetics experiments to calculate CBF. In the Kety model, the influence of diffusion on tracer movement is assumed to be negligible, and as a result the tracer concentrations in the intravascular space (IVS) and in the extravascular space (EVS) are assumed to be in diffusion equilibrium at all times. Any tracer that satisfies this description is referred to as a freely diffusible tracer, and using the approach described by Kety (1951), the operational equation is

$$Q(t) = F \int_0^t C_a(t-u) e^{-k_{1c}u} du \quad (1)$$

where all terms in Equation 1 are defined in Table 1 except the rate constant k_{1c} , which is defined as

$$k_{1c} = \frac{F}{\lambda} \quad (2)$$

Using nonlinear regression analysis, the Kety equation (Equation 1) with the measured arterial concentration, $C_a(t)$, is fitted to the tissue clearance data, $Q(t)$, to obtain an estimate of k_{1c} . Cerebral blood flow can then be determined from k_{1c} using a known value of λ (Herscovitch and Raichle, 1985).

Diffusion limitation of water

It has been demonstrated that water is not a freely diffusible tracer in the brain (Eichling et al., 1974), and as a result, the above relationship between F and k_{1c} has to be modified to include the extraction fraction (E) of water (Crone, 1963)

TABLE 1. Definition of terms

Symbol	Definition	Unit
IVS	Intra-vascular space	
EVS	Extra-vascular space	
α_j	Weighting factor for the j^{th} tissue compartment	$\text{mL} \cdot 100 \text{ g}^{-1} \cdot \text{min}^{-1}$
α_0	Vascular weighting factor	$\text{mL} \cdot 100 \text{ g}^{-1}$
λ	Equilibrium partition coefficient of tracer	$\text{mL} \cdot 100 \text{ g}^{-1}$
A_i	Cross-sectional area of IVS	$\text{cm}^2 \cdot 100 \text{ g}^{-1}$
A_e	Cross-sectional area of EVS	$\text{cm}^2 \cdot 100 \text{ g}^{-1}$
$C_i(x,t)$	Concentration of tracer in the IVS at time t and at some point x along the length of the capillary	mmole mL^{-1}
$C_e(t)$	Concentration of tracer in the EVS	mmole mL^{-1}
$C_a(t)$	Concentration of tracer in the arterial blood	mmole mL^{-1}
$C_v(t)$	Concentration of tracer in the venous blood	mmole mL^{-1}
C_0	Amount of tracer entering single capillary	mmole
F	Cerebral blood flow	$\text{mL} \cdot 100 \text{ g}^{-1} \cdot \text{min}^{-1}$
k_{1c}	Rate constant defined by Kety model	min^{-1}
k_{ad}	Rate constant defined by the adiabatic solution	min^{-1}
k_j	Rate constant for the j^{th} tissue type	min^{-1}
L	Length of capillary along the x -axis	cm
PS	Capillary permeability-surface area product	$\text{mL} \cdot 100 \text{ g}^{-1} \cdot \text{min}^{-1}$
$Q(t)$	Total amount of tracer in brain	$\text{mmole} \cdot 100 \text{ g}^{-1}$
$Q_i(t)$	Amount of tracer in the IVS	$\text{mmole} \cdot 100 \text{ g}^{-1}$
$Q_e(t)$	Amount of tracer in the EVS	$\text{mmole} \cdot 100 \text{ g}^{-1}$
T_c	Transit time through capillary	min
V_i	Distribution volume of tracer in the IVS	$\text{mL} \cdot 100 \text{ g}^{-1}$
V_e	Distribution volume of tracer in the EVS	$\text{mL} \cdot 100 \text{ g}^{-1}$

$$k_{ic} = \frac{EF}{\lambda} \tag{3}$$

where E represents the fraction of tracer that is extracted into the EVS during a single capillary transit. For modeling purposes, this fraction is assumed to attain an instantaneous diffusion equilibrium with the parenchymal tissue space (Kety, 1951). E is defined as (Crone, 1963)

$$E \equiv 1 - e^{-(PS/F)} \tag{4}$$

The Kety equation, after having been modified to include the extraction fraction of the tracer, becomes

$$Q(t) = EF \int_0^t C_a(t-u) e^{-k_{ic}u} du \tag{5}$$

where k_{ic} is now given by Equation 3.

There are two consequences to the diffusion limitation of water. First, because CBF is coupled with E , it is impossible to obtain an independent measurement of CBF from Equation 5 without knowing E . Depending on the magnitude of E , the underestimation of CBF can be significant if Equation 1 is used (Raichle et al., 1983). Second, Equation 5 does not account for the fact that the tracer (labeled water) requires a finite time to traverse the IVS. During this short time interval the entire amount of labeled water that enters at the arterial end of the capillary remains in the total tissue space (IVS and EVS). It has been demonstrated that the IVS tracer concentration can contribute to the signal and, if ignored, the CBF estimate may be time-dependent (Koeppel et al., 1987; Gambhir et al., 1987; Ohta et al., 1996).

Tissue homogeneity model

The TH model divides the brain into its two principal spaces: the IVS and the EVS, which are separated by the permeable blood-brain barrier (Johnson and Wilson, 1966; Sawada et al., 1989). Unlike the Kety model, the TH model defines the tracer concentration within the IVS as a function of both time and distance along the length of the capillary. Owing to the small radial dimension of a capillary, radial concentration gradients can be neglected. Within the EVS, the tracer concentration is assumed to be homogeneous (i.e., well mixed) in its spatial distribution, and therefore, within this space the TH model is compartmental. The TH model represents a simplified version of the one-barrier distributed-parameter model described by Goresky et al. (1973) and Larson et al. (1987). It has been postulated by Sawada et al. (1989) that because of the high density of capillaries in the brain and their tortuous arrangement, it may be justifiable to treat the EVS as a compartment.

The capillary-tissue unit as defined by the TH model is illustrated in Fig. 1. From conservation of the mass of tracer in both the IVS and the EVS, the following equations can be derived

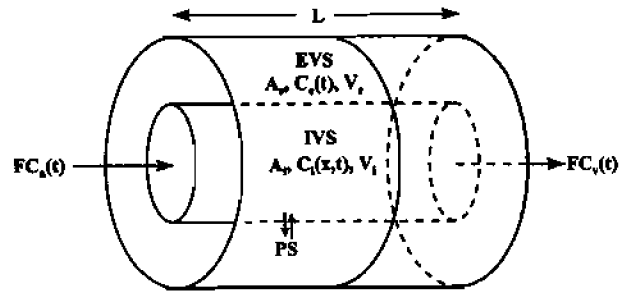


FIG. 1. The capillary-tissue unit as assumed by the tissue homogeneity model. The model is comprised of an intravascular space (IVS) surrounded by an extravascular space (EVS). Both spaces are of equal length, L , measured along the x axis, which is the direction of flow. The two spaces are separated by the blood-brain barrier, which has a permeability-surface area product denoted by PS . Both spaces have an associated cross-sectional area, A_i , volume V_i , and tracer concentration $C_i(t)$, where $k = i$ or e . The model assumes that only the IVS tracer concentration is a function of position. Blood flows into the capillary-tissue unit by means of the arterial blood at a flow rate F and concentration $C_a(t)$ and exits by means of the venous blood at the same flow rate and a concentration $C_v(t)$.

$$A_i \frac{\partial C_i(x,t)}{\partial t} = -F \frac{\partial C_i(x,t)}{\partial x} - \frac{PS}{L} \left[C_i(x,t) - \frac{C_e(t)}{\lambda} \right] \tag{6a}$$

$$A_e L \frac{dC_e(t)}{dt} = \frac{PS}{L} \int_0^L \left[C_i(x,t) - \frac{C_e(t)}{\lambda} \right] dx \tag{6b}$$

where all terms are defined in Table 1. These equations are subject to the following initial and boundary conditions

$$C_i(x,t=0) = C_e(t=0) = 0$$

$$C_i(x=0, t > 0) = C_0 \delta(t) \tag{7}$$

The formal solution to Equation 6 is provided in the subsection entitled "Solution to the Tissue Homogeneity Model" in the appendix.

Adiabatic approximation to the tissue homogeneity model

As shown in the appendix, the closed-form solution of the TH model exists only in Laplace space (Equations 23 and 24). In this section it is shown that an approximate closed-form solution in the time domain can be derived using the adiabatic approximation (Lassen and Perl, 1979). This approximation is motivated by the fact that the concentration of labeled water in the EVS ($C_e(t)$) changes slowly relative to that in the IVS ($C_i(t)$). Because of the difference in the time scale of these two events, for a small time interval, the slow event (i.e., the rate of change of $C_e(t)$) can be considered to be at a steady state while the fast event (i.e., the rate of change of $C_i(t)$) is taking place. The mathematical expression of the adiabatic approximation is to assume that within a small time increment (Δt), $C_e(t)$ is constant. This assumption is justified in the brain since, for water, the

ratio between its distribution volumes in the EVS and in the IVS is approximately 20:1 (Kety, 1951). Using the adiabatic assumption, $C_e(t)$ becomes discrete and is given formally as

$$C_e(t) = \sum_{j=0}^{n-1} \Delta C_e(j\Delta t) u(t - j\Delta t) \quad (8)$$

where $\Delta C_e(j\Delta t)$ is the discrete jump in the value of $C_e(t)$ at time $j\Delta t$, and $u(t)$ is the unit step function. A schematic diagram of this stepwise definition of $C_e(t)$ is illustrated in Fig. 2. The adiabatic solution to the TH model is derived by substituting Equation 8 for $C_e(t)$ in the differential Equations governing mass conservation (Equations 6a and 6b). The complete derivation of this solution is presented in the subsection entitled "Adiabatic Approximation to the Tissue Homogeneity Model" in the appendix.

For the TH model, the impulse residue function ($H(t)$) (Zieler, 1965) derived from the adiabatic approximation is given by

$$H(t) = 1 \quad 0 \leq t < T_c \quad (9a)$$

$$H(t) = E e^{-\frac{EF}{V_e}(t-T_c)} \quad t \geq T_c \quad (9b)$$

where $T_c = V_i/F$ is the transit time through the capillary and E is defined by Equation 4.

By comparing Equation 9 to Equation 23 and 24, we have demonstrated that $H(t)$ for the TH model can be greatly simplified by invoking the adiabatic approximation. With the adiabatic solution, $H(t)$ is divided into two phases in the time domain. For the vascular phase ($t < T_c$), $H(t)$ is equal to one owing to the finite time required for the labeled water to traverse the vascular space. During this phase, a fraction of the labeled water, denoted by E , is extracted into the EVS. At $t = T_c$, the remaining fraction ($1 - E$) exits by means of the outflowing blood, and hence there is a discrete drop in $H(t)$. For $t > T_c$, which is the parenchymal tissue phase of $H(t)$, the frac-

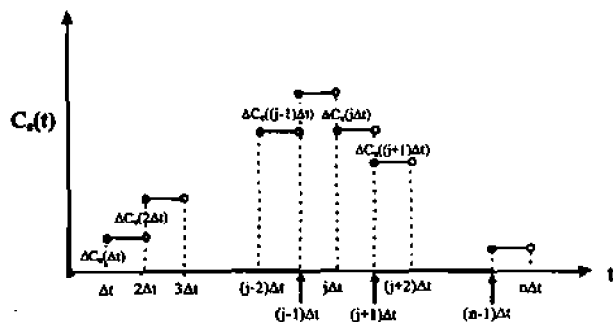


FIG. 2. A schematic representation of the adiabatic approximation. This approximation states that $C_e(t)$ can be represented by a staircase function because the EVS tracer concentration, $C_e(t)$, changes slowly relative to the IVS concentration, $C_i(x,t)$.

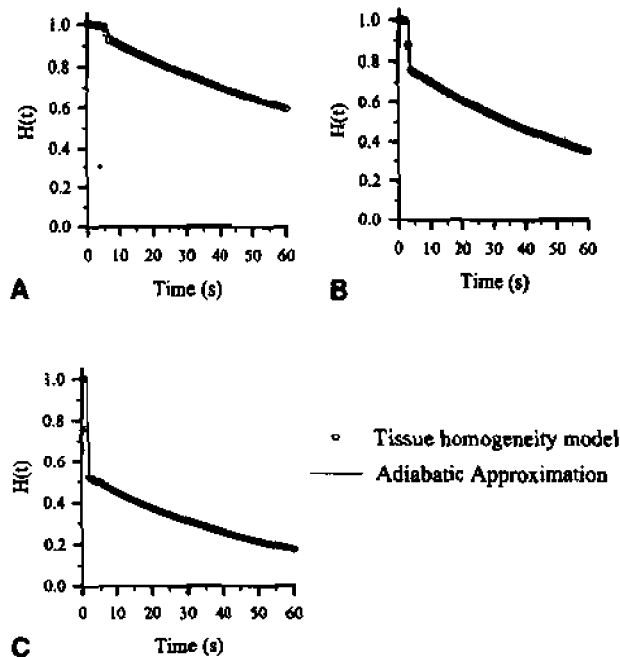


FIG. 3. The impulse residue function, $H(t)$, for the tissue homogeneity model as defined by the closed-form solution in the Laplace domain (Equations 23 and 24) compared with $H(t)$ derived using the adiabatic solution (Equation 9). The comparison is illustrated for three cases: (A) $CBF = 50 \text{ mL} \cdot 100 \text{ g}^{-1} \cdot \text{min}^{-1}$, (B) $CBF = 100 \text{ mL} \cdot 100 \text{ g}^{-1} \cdot \text{min}^{-1}$, and (C) $CBF = 200 \text{ mL} \cdot 100 \text{ g}^{-1} \cdot \text{min}^{-1}$. For all three cases shown, V_i , V_e , and PS were $4.0 \text{ mL} \cdot 100 \text{ g}^{-1}$, $94 \text{ mL} \cdot 100 \text{ g}^{-1}$, and $150 \text{ mL} \cdot 100 \text{ g}^{-1} \cdot \text{min}^{-1}$, respectively.

tion of labeled water extracted into the EVS diffuses back into the IVS and is removed by blood flow, leading to clearance from the parenchymal tissue compartment (EVS).

As a corollary to the adiabatic approximation, because the time rate of change of the concentration of labeled water in the IVS owing to blood flow is much faster than that owing to diffusion, the capillary acts as a sink for the labeled water leaving the EVS (by diffusion) during the parenchymal tissue phase. The rate of change of the tracer concentration in the EVS, which for the TH model is considered a well-stirred compartment, can then be expressed as

$$V_e \frac{dC_e(t)}{dt} = -EF C_e(t) \quad (10)$$

This equation has the same solution as derived for the TH model using the adiabatic approximation (Equation 9b). The product EF , as discussed by Renkin (1959) and Crone (1963), is the unidirectional flux of tracer from the EVS into the IVS.

Figure 3 plots the exact solution and the adiabatic solution for the impulse residue function of the TH model at three different values of CBF: (1) $50 \text{ mL} \cdot 100 \text{ g}^{-1} \cdot \text{min}^{-1}$, (2) $100 \text{ mL} \cdot 100 \text{ g}^{-1} \cdot \text{min}^{-1}$, and (3) 200

mL
mL
g⁻¹
Her
mer
app
Tiss
B
peri
arte
due
curv

I

Q(t)

B

the
rem

Q

wh
is in
t >
sho
reas

wh
k_{ad}

T
tiss
tion
com
con
CBF
wat
tiss
non
to t
V_i
I
dcri
time
tion
two

$\text{mL} \cdot 100 \text{ g}^{-1} \cdot \text{min}^{-1}$. The values of V_i , V_e , and PS were $4.0 \text{ mL} \cdot 100 \text{ g}^{-1}$, $94.0 \text{ mL} \cdot 100 \text{ g}^{-1}$, and $150 \text{ mL} \cdot 100 \text{ g}^{-1} \cdot \text{min}^{-1}$, respectively (Herscovitch and Raichle, 1985; Herscovitch et al., 1987). In all three cases, the agreement between the exact model solution and the adiabatic approximation was excellent.

Tissue residue curve

In CBF experiments, the tracer is often introduced at a peripheral site to avoid injection directly into a carotid artery. Under these conditions, the measured tissue residue curve $Q(t)$ is the convolution of $H(t)$ with an input curve $C_a(t)$ (Zierler, 1965)

$$Q(t) = F C_a(t) \otimes H(t) \quad (11)$$

Inserting Equation 9 into Equation 11, $Q(t)$ becomes

$$Q(t) = F \int_0^{T_c} C_a(t-u) du + EF \int_{T_c}^t C_a(t-u) e^{-\frac{EF}{V_e}(u-T_c)} du \quad (12)$$

By introducing the change of variable $u' = u - T_c$ in the second integral and by invoking the mean value theorem, Equation 12 can be written as

$$Q(t) = V_i C_a(t - \theta T_c) + EF \left[C_a(t') \otimes e^{-\frac{EF}{V_e} t'} \right] \quad (13)$$

where $V_i = FT_c$, $t' = t - T_c$, and $0 \leq \theta \leq 1$. Since T_c is in the order of a few seconds (Larson et al., 1987), for $t > T_c$ both $C_a(t)$ and the convolution term in Equation 13 should change minimally in $[(t - \theta T_c)t]$; therefore, it is reasonable to approximate Equation 13 as

$$Q(t) = V_i C_a(t) + EF [C_a(t) \otimes e^{-k_{adb} t}] \quad (14)$$

where the rate constant for the clearance of the tracer, k_{adb} , is defined as

$$k_{adb} = \frac{EF}{V_e} \quad (15)$$

The assumption that T_c is equal to 0 is necessary if the tissue residue curve is sampled with a temporal resolution equal to or greater than T_c . In the next section, computer simulations were performed to determine the consequences of using this assumption. To determine CBF from Equation 14, both the concentration of labeled water in arterial blood and the concentration in brain tissue must be determined for a given time duration. A nonlinear regression algorithm is used to fit Equation 14 to the brain tissue data with three fitting parameters: (1) V_i , (2) the product EF , and (3) the rate constant k_{adb} .

In summary, using the adiabatic approximation, we derived a closed-form solution to the TH model in the time domain. This solution is similar to the Kety equation for a diffusion-limited tracer (Equation 5) except for two differences. First, the definition of the rate constant

in the adiabatic solution involves V_e , whereas in the Kety equation, V_e is replaced by λ (Equation 3). In fact, V_e is equal to λ minus the distribution volume of water in the IVS, and therefore, these two parameters are similar in value in the brain. For example, in gray matter λ and V_e are equal to 98 and $94 \text{ mL} \cdot 100 \text{ g}^{-1}$, respectively (Herscovitch and Raichle, 1985). Second and more important, the adiabatic solution includes a vascular phase term, $V_i C_a(t)$, which accounts for the fact that during the transit time through the IVS (i.e., the vascular phase), the entire amount of tracer that enters by means of the arterial input remains in the tissue (both IVS and EVS). At the end of the vascular phase, at $t = T_c$, a fraction of it, $(1 - E)$, is removed by blood flow. It is the addition of the vascular phase term, $V_i C_a(t)$, that we believe will eliminate the FFP that has been reported in the past (Ginsberg et al., 1982; Raichle et al., 1983).

Solutions to two-compartment models, which are similar to the adiabatic solution of the TH model, have previously been proposed to account for the vascular signal contribution (Gambhir et al., 1987; Ohta et al., 1996; Takagi et al., 1984). A limitation to modeling the IVS as a compartment is that the concentration is assumed to be uniform throughout the capillary. If the tracer exhibits any finite extraction, then it will continuously diffuse into the EVS during its passage from the arterial to the venous end of the capillary. As a result, there will be a concentration gradient from the arterial end to the venous end, and the assumption of a uniform capillary concentration is violated. It is interesting to note that although the TH model begins with a more realistic description of the exchange of water between the capillary and extravascular tissue, under the adiabatic approximation it reduces to a solution similar to that derived from compartmental analysis (Ohta et al., 1996). Therefore our derivation has shown the similarity between two-compartment models and the TH model in modeling transcapillary exchange in the brain.

METHODS

Accuracy of the adiabatic solution

The results presented in Fig. 3 demonstrated the excellent agreement between the closed-form solution in Laplace domain of the TH model (Equations 23 and 24) and the closed-form solution in the time domain derived using the adiabatic approximation (Equation 9). The final step taken to arrive at Equation 14 was to assume that for the case of a tissue residue curve sampled with time intervals greater than T_c , the mean transit time was zero. Computer simulations were used to determine whether this assumption was permissible over a wide range of CBF values. Simulated tissue residue data were generated using Equation 12 and a model arterial blood curve (Fig. 4). This arterial blood curve was determined by fitting a sum of three gamma variate functions to a representative set of arterial blood data from a D_2O washout experiment (see Part II). For all simulations, PS was $150 \text{ mL} \cdot 100 \text{ g}^{-1} \cdot \text{min}^{-1}$ (Herscovitch et al., 1987), and the volumes of the blood space and parenchymal

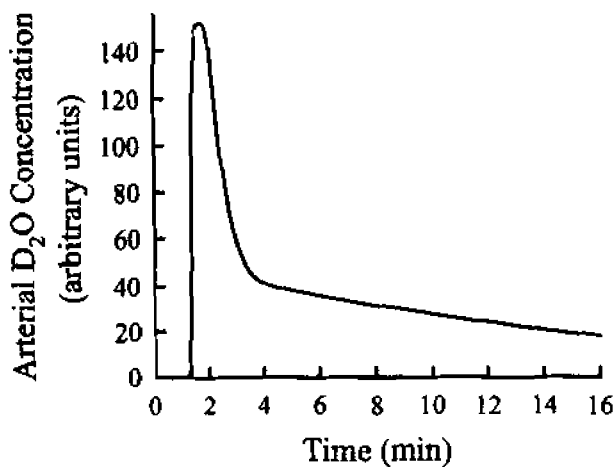


FIG. 4. The model curve of arterial blood D_2O concentration versus time, which was used for all statistical error analysis. This curve was obtained by fitting a sum of three gamma variate functions to the set of experimental data from an experiment in Part II.

tissue space were 4 and 94 mL $\cdot 100 \text{ g}^{-1}$, respectively (Herscovitch and Raichle, 1985). Each simulated data set for $Q(t)$ consisted of 900 data points with a sampling interval of 0.75 seconds for a total duration of 11.25 minutes. The simulated tissue data were generated over a range of flow values from 25 to 300 mL $\cdot 100 \text{ g}^{-1} \cdot \text{min}^{-1}$, and Equation 14 was fitted to the data using a quasi-Newton algorithm (Gill and Murray, 1974). Three fitting parameters were used in the analysis: (1) V_i , (2) the product EF , and (3) k_{adb} , as defined by Equation 15 because only one tissue type was simulated in these simulations.

Error analysis

Noise, present in both the data for the concentration of D_2O in arterial blood and for the concentration of D_2O in tissue, will affect the precision of the estimated parameters. The influence of noise in the two data sets was investigated using both the covariance matrix (COV) method (Huang et al., 1986) and Monte Carlo computer simulations. The COV method was used for the noise analysis with the tissue data since the COV method was far less time-consuming than Monte Carlo computer simulations. However, the latter approach had to be used for the analysis of noise in the arterial blood data because the COV method could not account for noise in the input data. Since the two noise sources were uncorrelated in the experiments outlined in Part II, the total standard deviation associated with a parameter was equal to the standard deviations from both analyses added in quadrature.

The error analysis was designed to reflect the ^2H clearance experiments that are described in Part II. For these experiments, the adiabatic solution (Equation 14) was summed over two tissue types because the surface coil detected the ^2H signal from both gray and white matter. The operational equation used in the simulations was as follows

$$Q(t) = \sum_{j=1}^2 \alpha_j \int_0^t C_a(t-u) e^{-k_j u} du + \alpha_b C_a(t) \quad (16)$$

where α_j and k_j represented the weighting factor and the rate constant, respectively, for the j th tissue type (gray or white matter). The weighting factor was dependent on the product EF of the tissue type, as in Equation 14, the relative fraction, and the spatial sensitivity of the surface coil for the tissue type, as discussed in Part II. Note that the subscript adb was dropped

from the rate constant since only its value was important for the error analysis and not its definition. The vascular phase terms for both tissue types had been lumped together as one ($\alpha_b C_a(t)$). The parameter α_b depended on the vascular volume, the relative fraction, and the spatial sensitivity of the surface coil for each tissue type, similar to the case with α_j . In the ^2H clearance experiments, it was not possible to cross-calibrate the two data sets ($Q(t)$ and $C_a(t)$) owing to the nonuniformity of the spatial sensitivity of the surface coil. Therefore, in these experiments it was only the rate constant k_j that was related to CBF in the j th tissue compartment and not the weighting factor α_j . For this reason we focused our attention primarily on the rate constants in these simulations.

In the analysis of the ^2H clearance data, a time shift (Δt) between the two data sets was included in the fitting routine to account for the difference between the arrival time of the labeled water in the brain and at the location at which the arterial blood was sampled. From a preliminary study we determined that including Δt as a fitting parameter had negligible effects on the precision and accuracy of the two rate constants. Since it was the rate constants that we were interested in, the parameter Δt was excluded from the error analysis. In summary, there were five regression parameters in the error analysis: two sets of α_j and k_j for gray and white matter, respectively, and α_b for the combined vascular phase terms of both gray and white matter. The SNR for each data set was defined as the maximum signal in a data set divided by the standard deviation of the background signal obtained from the spectra collected before D_2O injection (see Part II). The error analysis was performed using typical hypocapnia and normocapnia parameter values determined from the experiments described in Part II. These values are listed in Table 2, and the model arterial blood curve used in the analysis is illustrated in Fig. 4.

Using the COV method, the coefficient of variation (CV) of each of the parameters listed in Table 2, was determined over a range of SNR (50 to 150) in the tissue data. Very briefly, the COV is defined as (Huang et al., 1986)

$$\text{COV} = G^{-1} \quad (17)$$

where G is the information matrix, and the (ij)th element of this matrix is given by

$$g_{ij} = \sum_k \frac{\partial Q(t_k)}{\partial p_i} \cdot \frac{\partial Q(t_k)}{\partial p_j} \cdot \frac{1}{\text{var}_k} \quad (18)$$

where p_i refers to the i th parameter, and var_k is the noise variance of $Q(t_k)$. If the number of data points, $Q(t_k)$, is large, then the diagonal terms of the COV approximate the variances of the parameter estimates. For this error analysis, $Q(t)$ consisted of 300 samples with a sampling interval of 3 seconds, which was the data collection protocol used in the ^2H clearance experiments.

In the ^2H clearance experiments described in Part II, the data were also analyzed with the Kety equation summed over two tissue types to account for signals from both gray and white

TABLE 2. Hypocapnia and normocapnia parameter values

Parameters	Normocapnia	Hypocapnia
α_b (mL $\cdot 100 \text{ g}^{-1}$)	0.10	0.03
α_t (mL $\cdot 100 \text{ g}^{-1} \cdot \text{min}^{-1}$)	0.75	0.81
k_1 (min^{-1})	0.80	0.50
α_2 (mL $\cdot 100 \text{ g}^{-1} \cdot \text{min}^{-1}$)	0.15	0.16
k_2 (min^{-1})	0.20	0.10

matter in the brain (Equation 16 without the $\alpha_b C_a(t)$ term). The purpose there was to investigate the FFP by comparing the results from the Kety equation to those from the adiabatic solution. In the present study, to compare the precision of the two rate constants determined from the Kety equation with those from the adiabatic solution, the above error analysis was repeated by excluding the $\alpha_b C_a(t)$ term in Equation 16. These simulations were only performed for the normocapnia values listed in Table 2. From this comparison, the effect of introducing the variable α_b on the precision of the two rate constants was determined.

For the simulations with noise included in the arterial blood data, a theoretical tissue residue curve was generated using Equation 16 with the parameter values listed in Table 2 and the model arterial blood curve (Fig. 4) at a temporal resolution of 3 seconds. For each simulation, an arterial data set was generated from the model arterial curve using the sampling protocol followed in the ^2H clearance experiments described in Part II, which consisted of acquiring a sample every 6 seconds for the first 3.5 minutes, then every 12 seconds for the next 3 minutes, and finally every 30 seconds for the last 8.5 minutes. Noise was added to the arterial blood data, and before fitting Equation 16 to the theoretical tissue curve, the noisy arterial blood data set was interpolated to the same sampling interval as the tissue data. The Monte Carlo technique involved repeated simulations of the regression analysis with pseudorandom Gaussian noise added to the arterial data each time. The CV of each of the five parameters was determined from the distribution of estimated values generated from 500 simulations. The entire procedure was repeated for the same SNR range as was studied in the error analysis for noise in the tissue data.

Bias in the estimated parameters

Computer simulations were used to determine whether the correlation between the parameters could introduce a bias in the estimate of a parameter. The procedure for this study was analogous to the procedure for the simulations of noise in the arterial blood data except (1) the noise was added to the tissue data instead of the arterial blood data, (2) the SNR was maintained at 100, (3) simulations using the adiabatic solution (Equation 16) were generated only for the normocapnia parameters listed in Table 2, and (4) the simulations were performed for experimental durations of 4, 9, and 14 minutes. The same simulations were also conducted for the Kety equation summed over two tissue types. The only difference between the simulations for the Kety equation and those for the adiabatic solution was that the vascular phase term, α_b , in Equation 16 was set to zero for the former case. By comparing the results of the simulations for the adiabatic solution with the results for the Kety model, any bias introduced by a correlation between α_b and the rate constants will be evident since the simulations for the Kety model did not include α_b .

RESULTS

Accuracy of the adiabatic solution

The percent difference of the true values of the model parameters, EF and k_{adb} , from the estimated values, determined from regression analysis, is illustrated in Fig. 5A. For each parameter, the percent difference was plotted as a function of CBF. The estimated values of V_i from the regression analysis are presented in Fig. 5B. At all flow values investigated, the product EF was overestimated and V_i was consistently underestimated, both of

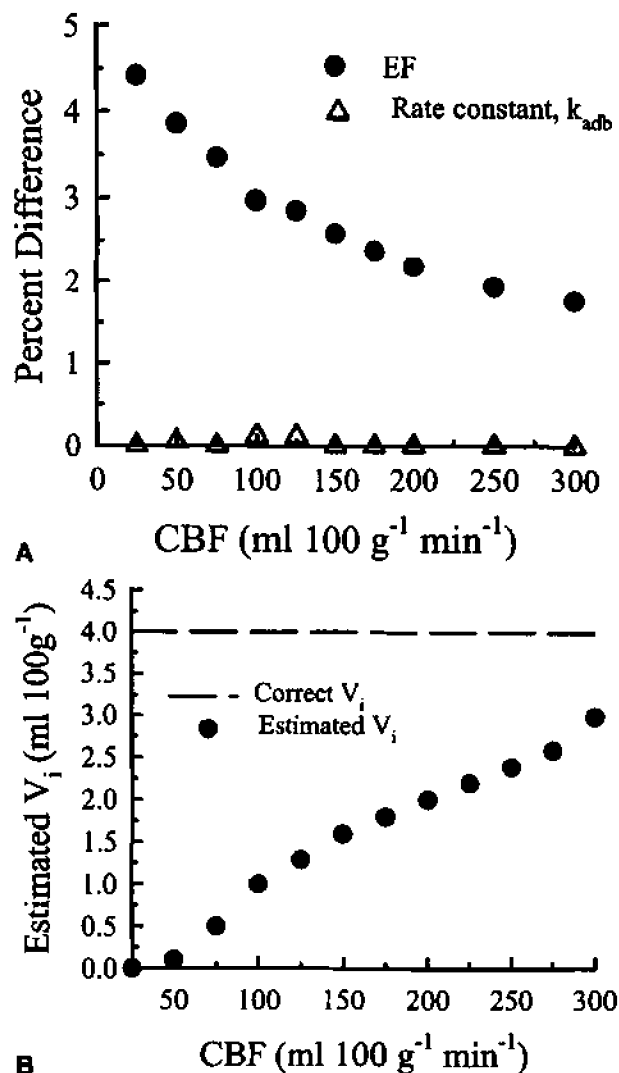


FIG. 5. The effect on estimates of parameters in the adiabatic solution of the tissue homogeneity model by assuming that the mean transit time is equal to zero. (A) The percent error in the estimates of the model parameters, EF and k_{adb} , as a function of CBF. (B) Estimates of the parameter V_i as a function of CBF. All simulated tissue residue curves were generated using the arterial blood curve illustrated in Fig. 4 and the following values for the parameters V_i , V_o , and PS : 4.0 mL·100 g⁻¹, 94 mL·100 g⁻¹, and 150 mL·100 g⁻¹·min⁻¹, respectively.

which were attributed to setting T_c equal to 0 in Equation 13. To understand these results, it should be noted that the vascular phase term for the adiabatic solution originates from the integration of the arterial concentration of the tracer from time 0 to T_c . As well, the integration limits of the second term of Equation 12, which represents the fraction of labeled water extracted into parenchymal tissue, are from T_c to t . By forcing T_c to be 0, the fitting parameter V_i in Equation 14 could not account for the total area of the vascular phase term in Equation 12. Likewise, because the integration for the second term in Equation 14 is from 0 to t , EF therefore includes a por-

tion of the vascular phase term in Equation 12. The accuracy of k_{ad} is not affected by this assumption because T_c does not contribute to the rate of tracer clearance from the EVS.

Error analysis

Figure 6A illustrates the CV of the rate constant, k_1 , of the higher flow tissue compartment (gray matter) as a function of SNR for four conditions: (1) hypocapnia with noise added to the tissue data, (2) hypocapnia with noise added to the arterial data, (3) normocapnia with noise added to the tissue data, and (4) normocapnia with noise added to the arterial data. The parameters for the hypocapnia and normocapnia simulations are given in Table 2. In Fig. 6B, the CV of the rate constant, k_2 , of the lower flow tissue compartment (white matter) is plotted as a function of SNR for the same four conditions as for k_1 . Because CBF was determined only from the rate constants, the CV of the other fitting parameters were not presented. The results in Fig. 6 indicated that the effect of noise in the arterial data was greater than that of the noise in the tissue data for the same SNR value. This difference could be attributed to the fact that fewer data points were acquired for the arterial data compared with the tissue data (70 versus 300, respectively).

For all of the ^2H clearance experiments, the SNR of the arterial blood data ranged from 70 to 100 and that of the tissue data was always greater than 120. For these SNR values, the CV of k_1 would be approximately 6% owing to noise in the arterial data and 3% owing to noise in the tissue data. If the standard deviations were assumed to add in quadrature, then the total CV of k_1 was 6.7%. The precision of k_2 was considerably worse than that of k_1 . For the same SNR values, the CV of k_2 was roughly 20% for the arterial blood data and 10% for the tissue data, for a total CV of 22%. This reduction in the precision of k_2 was attributed to the smaller weighting factor for the second compartment. The importance of these precision estimates to the CBF measurements obtained with the ^2H clearance technique will be addressed in the accompanying paper.

Besides the adiabatic solution simulations above, simulations involving the Kety equation were conducted to determine the decrease in precision that could be expected by including the additional term α_b in the regression analysis. In Fig. 7, the CV for k_1 and k_2 are presented for both the adiabatic solution and the Kety equation summed over two tissue types. These simulations included only noise in the tissue data. As shown in these figures, including α_b resulted in an increase of no greater than 3% for the CV of either rate constant over the entire range of SNR values studied.

Bias in the estimated parameters

In Table 3, the mean k_1 and k_2 values from 500 simulations with noise added to the tissue data are listed. The

results of the simulations of both the Kety equation and the adiabatic solution for three different experimental durations, 4, 9, and 14 minutes, were presented. The true values of k_1 and k_2 were the normocapnia values listed in Table 2. These results indicated that when only the first 4 minutes of the data were included in the regression analysis, both rate constants were overestimated with either the Kety model or the adiabatic solution. Furthermore, this bias was more pronounced with the higher rate constant, k_1 , than with the lower rate constant, k_2 . The bias was significantly larger for the adiabatic solution, which was attributed to the correlation between α_b and

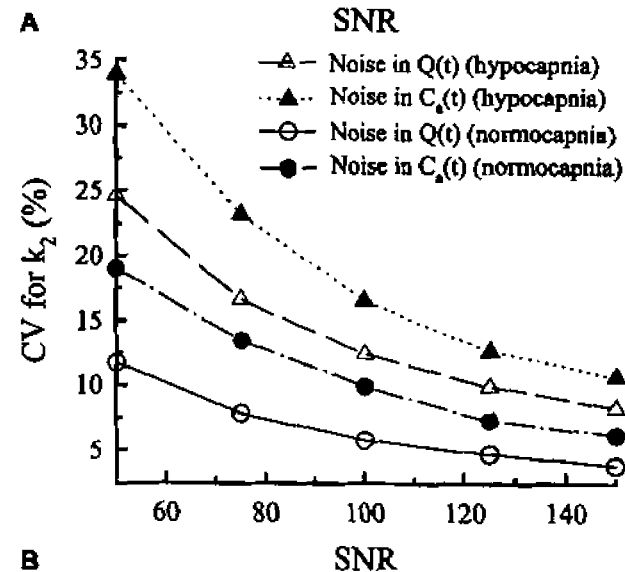
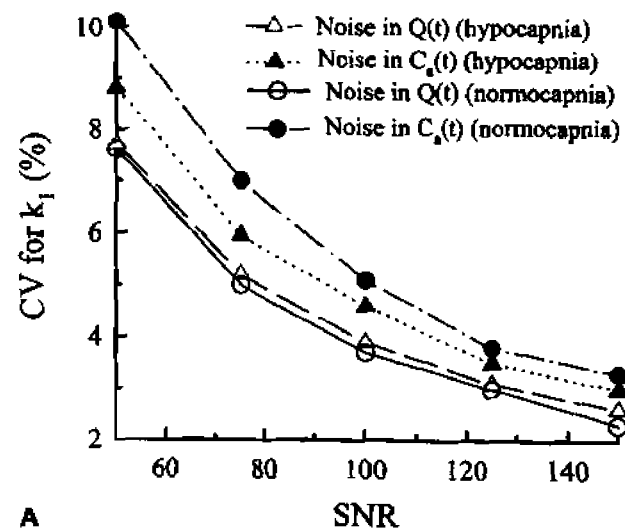


FIG. 7. (A) The coefficient of variation for k_1 plotted as a function of SNR. The parameter values used in the error analysis are listed in Table 2. Four different conditions are illustrated: (1) hypocapnia with noise added to the tissue data (dashed line with open triangles), (2) hypocapnia with noise added to the arterial data (dotted line with filled triangles), (3) normocapnia with noise added to the tissue data (solid line with open circles), and (4) normocapnia with noise added to the arterial data (dashed-dotted line with filled circles). (B) The CV for k_2 plotted as a function of SNR for the same four conditions as listed for k_1 .

CV for k_1 (%)

A

CV for k_2 (%)

B

FIG. 7.
SNR. T
TH mo
erated
moco
funcio

k_1 . By
this co
bias in
bias w
sence
model
fitting

In t
closed
using
this de
can be
data b
more,
eters
it can
resolu
tions
studies
magne

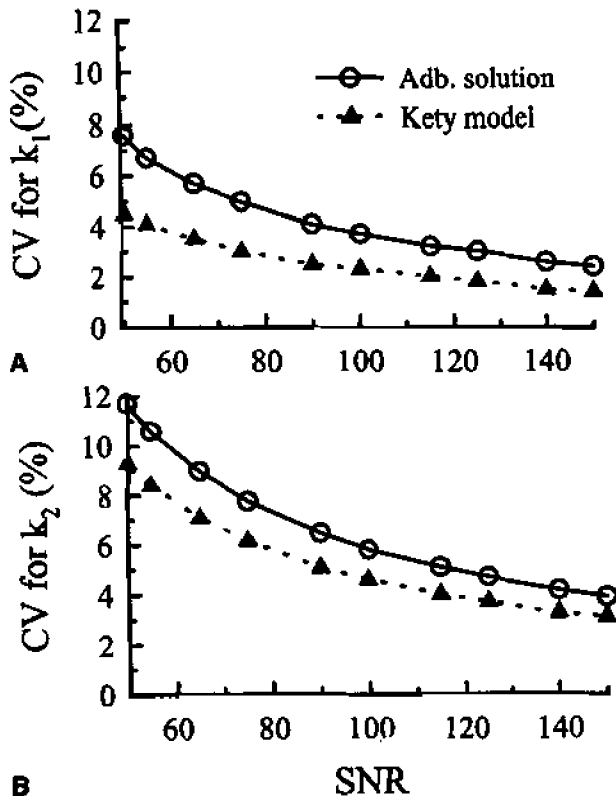


FIG. 7. (A) The CV for k_1 plotted as a function of tissue data SNR. The CV is presented for both the adiabatic solution of the TH model and the Kety model solution. These results were generated using the parameter values listed in Table 2 for the normocapnia case. (B) The corresponding CV for k_2 plotted as a function of the tissue data SNR.

k_1 . By increasing the experimental duration to 9 minutes, this correlation was sufficiently reduced such that the bias in k_1 was eliminated. With the Kety equation, the bias was not nearly as large simply because of the absence of α_p . The small bias associated with the Kety model was attributed to the constraints imposed on the fitting parameters in the regression analysis.

DISCUSSION

In this study it was demonstrated that a time-domain, closed-form solution to the TH model can be derived using the adiabatic approximation. The consequences of this derivation are twofold. First, the adiabatic solution can be easily implemented in the analysis of clearance data because the solution is in the time domain. Furthermore, considering that there are only three fitting parameters (V_i , EF , and k_{adb}) in the model for each tissue type, it can be used to analyze clearance data of limited time resolution or SNR, or both. Examples of such applications include dynamic positron emission tomography studies with the tracer $H_2^{15}O$ (Alpert et al., 1984) and magnetic resonance spectroscopy using the tracer D_2O

(Kim and Ackerman, 1990). Second, the similarity between the adiabatic solution and the solutions derived from two-compartment models indicates that the use of two-compartment models is reasonable provided that the vascular phase of the signal is properly accounted for in the models.

Using computer simulations, the accuracy of the adiabatic solution (Equation 14) was investigated over a wide range of CBF values (25 to 300 mL/100 g $^{-1}$ ·min $^{-1}$). It was determined that the assumption $T_c = 0$ results in a consistent underestimation of V_i and an overestimation of EF ; however k_{adb} remains unaffected. These results are significant for two reasons. First, the accuracy of the CBF measurements presented in Part II was not compromised by this approximation since CBF was determined from k_{adb} only. Second, these findings suggest that the measured product EF could not be considered to represent only water clearance from the EVS (Ohta et al., 1996), since this parameter might be overestimated for reasons discussed in the Results section. However, this overestimation would not be as large as when the vascular phase term is ignored completely (Ohta et al., 1996). Finally, the assumption that T_c is equal to zero is only necessary to accommodate clearance data collected with limited temporal resolution. If the data are acquired with sufficient temporal resolution (i.e., sampling interval less than T_c), then T_c can be included as a fitting variable in the regression analysis, which will avoid these errors.

Although the results illustrated in Fig. 3 clearly demonstrated the validity of the adiabatic solution to the TH model, they were only generated for parameter values that reflect water transport in the brain. If another tracer is used or a different tissue studied, then it may be necessary to reevaluate the adiabatic solution under those specific conditions. Furthermore, the ability of the adiabatic solution to properly characterize tracer transport through the microvasculature depends on the validity of the TH model in representing the tissue studied. The variability of the microvascular architecture from one tissue type to another is considerable, and for some tissues, the representation of the EVS as a well-stirred compartment, as in the TH model, may not be valid. For instance, the highly ordered arrangement of the capillaries in the liver would mean that the EVS can not be represented by a compartment. It has been suggested that the TH model may not even be appropriate for characterizing water exchange in the brain (Kassissia et al., 1995), which in turn would cast doubt on the validity of the adiabatic solution. We have tested the validity of the adiabatic solution by measuring CBF in rabbit brain using magnetic resonance spectroscopy with the tracer D_2O and demonstrated that the TH model is valid for brain tissue. The results of this study will be presented in Part II.

TABLE 3. Mean k_1 and k_2 values from 500 simulations with noise added to the tissue data

Experimental duration (min)	Adiabatic solution		Kety model	
	mean k_1 (min^{-1}) [true $k_1 = 0.8$]	mean k_2 (min^{-1}) [true $k_2 = 0.2$]	mean k_1 (min^{-1}) [true $k_1 = 0.8$]	mean k_2 (min^{-1}) [true $k_2 = 0.2$]
4	1.51	0.24	1.07	0.23
9	0.80	0.20	0.80	0.20
14	0.80	0.20	0.80	0.20

As well as determining the accuracy of the adiabatic solution, the precision of the estimated model parameters was also investigated for the specific conditions of the experiments outlined in Part II. The error analysis involved summing the adiabatic solution over two tissue types because in the CBF experiments, the ^2H signal originated from both gray and white matter in the brain. Accounting for both tissue types greatly increased the demands on the SNR and the temporal resolution of the data. The results plotted in Fig. 6 demonstrated that the precision of the higher rate constant of the gray matter was acceptable. However, the precision of the lower rate constant of the white matter was poor because of its smaller weighting factor. By including the vascular phase term, α_b , in the regression analysis, a maximum of only 3% increase in the CV for either rate constant was determined. Therefore, the limiting factor for precision in the experimental protocol was summing the operational equation over two tissue types and not including α_b . Although α_b did not greatly increase the CV of either rate constant, it did introduce a bias in their estimated values, which was especially prominent for k_1 . However, the correlation between these parameters could be eliminated by increasing the experimental duration to greater than 9 minutes. As a result, for the CBF experiments discussed in Part II the time duration was chosen to be 15 minutes.

APPENDIX

Solution to the tissue homogeneity model

The formal solution to Equation 6 is obtained by using the Laplace transform. The transformed functions are denoted by a bar.

$$\bar{C}_i(x,s) = \int_0^\infty e^{-st} C_i(x,t) dt \quad (19)$$

$$\bar{C}_e(s) = \int_0^\infty e^{-st} C_e(t) dt \quad (20)$$

In terms of the transformed functions, Equations 6a and 6b can be rewritten as

$$s\bar{C}_i(x,s) + \frac{FL}{V_i} \frac{\partial \bar{C}_i(x,s)}{\partial x} + \frac{PS}{V_i} \left[\bar{C}_i(x,s) - \frac{1}{\lambda} \bar{C}_e(s) \right] = 0 \quad (21)$$

$$V_e s \bar{C}_e(s) - \frac{PS}{L} \int_0^L \bar{C}_i(x,s) dx - \frac{PS}{\lambda} \bar{C}_e(s) = 0 \quad (22)$$

The solutions of these equations are (Johnson and Wilson, 1966)

$$\bar{C}_i(x,s) = \frac{C_0}{s} e^{-(\alpha+\beta s)x/L} + \frac{[1 - e^{-(\alpha+\beta s)}] [1 - e^{-(\alpha+\beta s)x/L}]}{s[U(s) - e^{-(\alpha+\beta s)}]} \quad (23)$$

$$\bar{C}_e(s) = \frac{\lambda(\alpha + \beta s)[1 - e^{-(\alpha+\beta s)}]}{\alpha\beta s[U(s) - e^{-(\alpha+\beta s)}]} \quad (24)$$

where $U(s)$, a cubic polynomial in seconds, and the three variables, α , β , and χ , are defined as

$$U(s) = \frac{\chi}{\alpha^2} (\beta s)^3 + \frac{(2\chi + 1)}{\alpha} (\beta s)^2 + (\chi + 1)\beta s + 1$$

$$\alpha = \frac{PS}{F}, \beta = \frac{V_i}{F}, \chi = \frac{V_e}{V_i} \lambda \quad (25)$$

Adiabatic approximation to the tissue homogeneity model

To solve the mass conservation equations (Equations 6a and 6b) using the adiabatic approximation, we begin with the differential equation for the IVS. First, by Laplace transform with respect to time, Equation 6a can be written as follows

$$s\bar{C}_i(x,s) + \frac{FL}{V_i} \frac{\partial \bar{C}_i(x,s)}{\partial x} + \frac{PS}{V_i} \left[\bar{C}_i(x,s) - \sum_{k=0}^{n-1} \frac{\Delta C_e(k\Delta t) e^{-k\Delta t s}}{\lambda s} \right] = 0 \quad (26)$$

where the discrete version of $C_e(t)$, Equation 8, has been used. Next, Laplace transform with respect to position is performed by using the definition

$$\bar{\bar{C}}_i(p,s) = \int_0^\infty e^{-px} C_i(x,t) dx \quad (27)$$

where the double bar notation refers to the two Laplace transforms with respect to the variables x and t . The Laplace transform of Equation 26 with respect to position is

$$s\bar{C}_i(p,s) + \frac{FL}{V_i} p\bar{C}_i(p,s) - \frac{FL}{V_i} C_o + \frac{PS}{V_i} \left[\bar{C}_i(p,s) - \sum_{k=0}^{n-1} \frac{\Delta C_e(k\Delta t)e^{-k\Delta t s}}{\lambda_e p s} \right] = 0. \quad (28)$$

This equation is obtained using the boundary conditions stated in Equation 7. Performing the inverse Laplace transform with respect to p , we obtain the following equation

$$\bar{C}_i(x,s) = \sum_{k=0}^{n-1} \Delta' C_e(k\Delta t) \left[\frac{e^{-k\Delta t s}}{s} - \frac{e^{-k\Delta t s}}{s + \frac{PS}{V_i}} \right] + C_o e^{-\frac{V_i}{FL} x} - \frac{PS}{FL} x + C_o e^{-\frac{PS}{FL} x} - \frac{PS}{FL} x - \sum_{k=0}^{n-1} \Delta' C_e(k\Delta t) e^{-\frac{PS}{FL} x} \left[\frac{e^{-\left(k\Delta t + \frac{V_i x}{FL}\right) s}}{s} - \frac{e^{-\left(k\Delta t + \frac{V_i x}{FL}\right) s}}{s + \frac{PS}{V_i}} \right]. \quad (29)$$

In Eq. (29), we have made the substitution $\frac{\Delta C_e(k\Delta t)}{\lambda} = \Delta' C_e(k\Delta t)$. Next we perform the inverse Laplace transform with respect to t :

$$C_i(x,t) = \sum_{k=0}^{n-1} \Delta' C_e(k\Delta t) u(t - k\Delta t) - \sum_{k=0}^{n-1} \Delta' C_e(k\Delta t) e^{-\frac{PS}{V_i}(t-k\Delta t)} u(t - k\Delta t) - \sum_{k=0}^{n-1} \Delta' C_e(k\Delta t) e^{-\frac{PS}{FL} x} u\left(t - k\Delta t - \frac{V_i x}{FL}\right) + \sum_{k=0}^{n-1} \Delta' C_e(k\Delta t) e^{-\frac{PS}{FL} x} u\left(t - k\Delta t - \frac{V_i x}{FL}\right) + e^{-\frac{PS}{V_i}\left(t - k\Delta t - \frac{V_i x}{FL}\right)} + C_o e^{-\frac{PS}{FL} x} \delta\left(t - \frac{x}{v}\right). \quad (30)$$

where: $v = \frac{FL}{V_i}$.

Now consider one of the Δt intervals in $[0, n\Delta t)$, say $t \in [l\Delta t, (l+1)\Delta t)$, where $0 \leq l \leq (n-1)$. After some simplification Equation 30 becomes

$$C_i(x,t) = \sum_{k=0}^{l-1} \Delta' C_e(k\Delta t) \left[1 - e^{-\frac{PS}{FL} x} \right] + \Delta' C_e(l\Delta t) \left[e^{-\frac{PS}{FL} x} - e^{-\frac{PS}{V_i}(t-l\Delta t)} \right] \left[1 - u\left(t - \frac{x}{v} - l\Delta t\right) \right] + \Delta' C_e(l\Delta t) \left[1 - e^{-\frac{PS}{FL} x} \right] + C_o e^{-\frac{PS}{FL} x} \delta\left(t - \frac{x}{v}\right). \quad (31)$$

The next step is to integrate this equation over the length of the capillary to determine the amount of tracer in the IVS

$$Q_i(l\Delta t) = \left[A_i \int_0^L C_i(x,t) dx \right]_{t=l\Delta t} \quad (32)$$

Using Equation 31 to define $C_i(x,t)$, we obtain the following

$$Q_i(l\Delta t) = V_i C_e((l-1)\Delta t) - \frac{EF}{PS} V_i C_e((l-1)\Delta t) + C_o F e^{-\frac{PS}{V_i} l\Delta t} \quad 1 \leq l \leq m-1 \quad (33)$$

$$Q_i(l\Delta t) = V_i C_e((l-1)\Delta t) - \frac{EF}{PS} V_i C_e((l-1)\Delta t) \quad m \leq l \leq n-1, \quad (34)$$

for $t \in [l\Delta t, (l+1)\Delta t)$, where $C_e(l\Delta t) = \sum_{k=0}^l \Delta' C_e(k\Delta t)$ and

$m\Delta t = \frac{L}{v}$. In Eq. (A.12) the term E represents the extraction fraction of tracer as defined by Eq. (4).

With the tracer amount in the IVS known, the next step is to determine the tracer concentration in the EVS. Using Equation 31, the differential equation for tracer mass conservation in the EVS (Equation 6b) becomes

$$V_e \frac{dC_e(t)}{dt} = \frac{PS C_e(l\Delta t)}{\lambda} - EF C_e(l\Delta t) + (EF - PS) \Delta' C_e(l\Delta t) + C_o \frac{FPS}{V_i} e^{-\frac{PS}{V_i} t} [1 - u(t - m\Delta t)] - \frac{PS}{\lambda} C_e(t). \quad (35)$$

With the adiabatic approximation for $C_e(t)$, we could assume $C_e(l\Delta t) = C_e(t)$ for $t \in [l\Delta t, (l+1)\Delta t)$, and hence Equation 35 becomes

$$V_e \frac{dC_e(t)}{dt} + EF C_e(l\Delta t) = (EF - PS) \Delta' C_e(l\Delta t) + C_o \frac{FPS}{V_i} e^{-\frac{PS}{V_i} t} \quad l \leq m-1, \quad (36)$$

$$V_e \frac{dC_e(t)}{dt} + EF C_e(l\Delta t) = (EF - PS) \Delta' C_e(l\Delta t) \quad l \geq m. \quad (37)$$

Equation 36 has the solution

$$C_e((l+1)\Delta t) = C_e(l\Delta t) e^{-\frac{EF}{V_e} \Delta t} + \frac{f_l(t-l\Delta t) * e^{-\frac{EF}{V_e} \Delta t}}{V_e} + e^{-\frac{PS}{V_i} l\Delta t} C_e(\Delta t), \quad (38)$$

where * denotes the convolution operator and the factor f_1 is defined as

$$f_1(t-l\Delta t) = EF\Delta' C_e(l\Delta t) - F\Delta' C_e(l\Delta t) + \Delta' C_e(l\Delta t) e^{-\frac{PS}{V_i}(t-l\Delta t)} \left[F - PS + \frac{FPS}{V_i}(t-l\Delta t) \right]. \tag{39}$$

For an infinitesimally small Δt , the convolution will approach zero and thus Equation 38 reduces to

$$C_e((l+1)\Delta t) = C_e(l\Delta t)e^{-\frac{EF}{V_e}\Delta t} + e^{-\frac{PS}{V_i}l\Delta t} C_e(\Delta t) \quad l \leq m-1. \tag{40}$$

Similarly, the solution to Equation 37 is

$$C_e((l+1)\Delta t) = C_e(l\Delta t)e^{-\frac{EF}{V_e}\Delta t} \quad l \geq m. \tag{41}$$

From these recursive relationships, Equations 40 and 41, it can be shown that for any interval k the EVS concentration is given by

$$C_e(k\Delta t) = \frac{C_o F e^{-\frac{EF}{V_e}k\Delta t}}{V_e \Gamma} \left[1 - e^{-\frac{PS}{V_i}\Gamma k\Delta t} \right] \quad 0 \leq k < m-1 \tag{42}$$

$$C_e(k\Delta t) = \frac{C_o F e^{-\frac{EF}{V_e}k\Delta t}}{V_e \Gamma} \left[1 - e^{-\frac{PS}{F}\Gamma} \right] \quad m \leq k < n-1, \tag{43}$$

where $\Gamma = 1 - \frac{EFV_i}{PSV_e}$.

Using Equations 42 and 43 to define the EVS concentration, the amount of tracer in the IVS can be determined from Equations 33 and 34.

$$Q_i(k\Delta t) = C_o F \left(1 - \frac{1}{\Gamma} \left(1 - \frac{V_i}{V_e} \right) \right) e^{-\frac{EF}{V_e}k\Delta t} \left[1 - e^{-\frac{PS}{V_i}\Gamma k\Delta t} \right] + C_o F e^{-\frac{PS}{V_i}k\Delta t} \quad 1 \leq k < m-1 \tag{44}$$

$$Q_i(k\Delta t) = C_o F \left(1 - \frac{1}{\Gamma} \left(1 - \frac{V_i}{V_e} \right) \right) e^{-\frac{EF}{V_e}k\Delta t} \left[1 - e^{-\frac{PS}{F}\Gamma} \right] \quad m \leq k \leq n-1. \tag{45}$$

The total amount of tracer in the brain volume is given by

$$Q(t) = V_e C_e(t) + Q_i(t). \tag{46}$$

From Equations 42, 43, 44, and 45, $Q(t)$ is

$$Q(k\Delta t) = C_o F \left(1 + \frac{V_i}{\Gamma V_e} \right) e^{-\frac{EF}{V_e}k\Delta t} \left[1 - e^{-\frac{PS}{V_i}\Gamma k\Delta t} \right] + C_o F e^{-\frac{PS}{V_i}k\Delta t} \quad 1 \leq k < m-1 \tag{47}$$

$$Q(k\Delta t) = C_o F \left(1 + \frac{V_i}{\Gamma V_e} \right) e^{-\frac{EFV_i}{V_e}k\Delta t} \left[1 - e^{-\frac{PS}{F}\Gamma} \right] e^{-\frac{EF}{V_e}(k-m)\Delta t} \quad m \leq k \leq n-1. \tag{48}$$

These equations can be simplified considerably by making the following assumptions: (i) $\Gamma \sim 1$ since $EFV_i \ll$

PSV_e (ii) in Eq. (47) $e^{-\frac{EF}{V_e}k\Delta t} - 1$ since $k\Delta t$ is less than or equal to the capillary transit time, and (iii) in Eq.

(A.48) $e^{-\frac{EFV_i}{V_e}k\Delta t} - 1$ since $V_e \gg EV_i$. Therefore,

$$\left(1 + \frac{V_i}{\Gamma V_e} \right) e^{-\frac{EF}{V_e}k\Delta t} \left[1 - e^{-\frac{PS}{V_i}\Gamma k\Delta t} \right] + e^{-\frac{PS}{V_i}k\Delta t} = 1 \quad 1 \leq k < m-1 \tag{49}$$

$$\left(1 + \frac{V_i}{\Gamma V_e} \right) e^{-\frac{EFV_i}{V_e}k\Delta t} \left[1 - e^{-\frac{PS}{F}\Gamma} \right] = \left[1 - e^{-\frac{PS}{F}} \right] \quad m \leq k \leq n-1. \tag{50}$$

To demonstrate the validity of these approximations, the terms on the left side of Equations 49 and 50 and their respective approximate solutions (the right side of the equations) are plotted as functions of CBF in Fig. 8. For these curves, values of V_i , V_e , and PS are chosen that represent typical values for water transport in brain: 4.0 mL·100 g⁻¹, 94.0 mL·100 g⁻¹, and 150 mL·100 g⁻¹·min⁻¹, respectively (Herscovitch and Raichle, 1985; Herscovitch et al., 1987). Equation 49 is plotted for a transit time of 3 seconds, which represents the mean

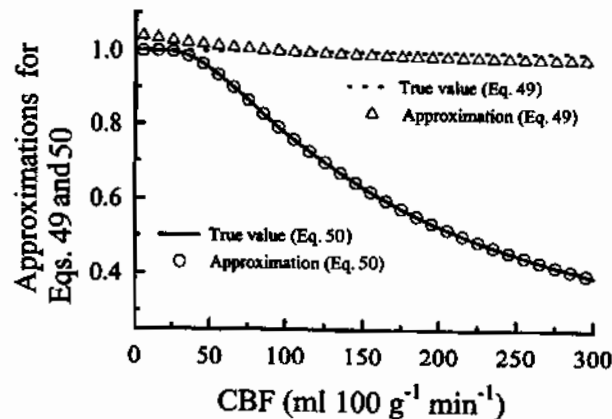


FIG. 8. Graphical representation of the approximations given by Equations 49 and 50 plotted as a function of CBF. For all calculations, V_i , V_e , and PS were 4.0 mL·100 g⁻¹, 94.0 mL·100 g⁻¹, and 150 mL·100 g⁻¹·min⁻¹, respectively. Equation 49 was plotted for a transit time of 3 seconds.

vasc
impu
equa
mati
H(t)
tion.

Alper
J,
n
tr
2:
Corbe
m
d
B
Crone
d
io
Detre
Z
fl
M
Eichli
E
br
Frackl
m
lis
pr
Gambi
th
of
to
Gill Pl
m
Ginsbe
IE
eg
itr
tic
Goresl
by
Cl
Hersoc
br
M
Hersoc
m
pr
Bl

vascular transit time in brain (Larson et al., 1987). The impulse residue function, $H(t)$, is obtained by setting C_0F equal to 1 in Equations 47 and 48 and using the approximations given in Equations 49 and 50. The final form of $H(t)$ is shown in Equations 9a and 9b in the theory section.

REFERENCES

- Alpert NM, Eriksson L, Chang JY, Bergstrom M, Litton JE, Correia JA, Bohm C, Ackerman RH, Taveras JM (1984) Strategy for the measurement of regional cerebral blood flow using short-lived tracers and emission tomography. *J Cereb Blood Flow Metab* 4: 28-34
- Corbett RJT, Lupton AR, Olivares E (1991) Simultaneous measurement of cerebral blood flow and energy metabolites in piglets using deuterium and phosphorus nuclear magnetic resonance. *J Cereb Blood Flow Metab* 11:55-65
- Crone C (1963) The permeability of capillaries in various organs as determined by use of the 'indicator diffusion' method. *Acta Physiol Scand* 58:292-305
- Detre JD, Subramanian VH, Mitchell MD, Smith DS, Kobayashi A, Zaman A, Leigh JS (1990) Measurement of regional cerebral blood flow in cat brain using intracarotid $^2\text{H}_2\text{O}$ and ^2H NMR imaging. *Magn Reson Med* 14:389-395
- Eichling JO, Grubb RL Jr, Raichle ME, Ter-Pogossian MM (1974) Evidence of the limitations of water as a freely diffusible tracer in brain of the rhesus monkey. *Circulation Res* 35:358-364
- Frackowiak RSJ, Lenzi G-L, Jones T, Heather JD (1980) Quantitative measurement of regional cerebral blood flow and oxygen metabolism in man using O-15 and positron emission tomography: theory, procedure, and normal values. *J Comput Assist Tomogr* 4:727-736
- Gambhir SS, Huang S-C, Hawkins RA, Phelps ME (1987) A study of the single compartment tracer kinetic model for the measurement of local cerebral blood flow using ^{15}O -water and positron emission tomography. *J Cereb Blood Flow Metab* 7:13-20
- Gill PE, Murray W (1974) *Numerical Methods for Constrained Optimization*, London, Academic Press
- Ginsberg MD, Lockwood NH, Busto R, Finn RD, Bulter CM, Cendan IE, Goddard J (1982) A simplified *in vivo* autoradiographic strategy for the determination of regional cerebral blood flow by positron emission tomography: theoretical considerations and validation studies in the rat. *J Cereb Blood Flow Metab* 2:89-98
- Goresky CA, Bach GG, Nadeau BE (1973) On the uptake of materials by the intact liver. The transport and net removal of galactose. *J Clin Invest* 52:991-1009
- Herscovitch P, Raichle ME (1985) What is the correct value for the brain-blood partition coefficient for water? *J Cereb Blood Flow Metab* 5:65-69
- Herscovitch P, Raichle ME (1987) Positron emission tomographic measurement of cerebral blood flow and permeability-surface area product of water using ^{15}O water and ^{11}C butanol. *J Cereb Blood Flow Metab* 7:527-542
- Huang S-C, Carson RE, Phelps ME (1982) Measurement of local blood flow and distribution volume with short-lived isotopes: a general input technique. *J Cereb Blood Flow Metab* 2:99-108
- Huang S-C, Feng D, Phelps ME (1986) Model dependency and estimation reliability in measurement of cerebral oxygen utilization rate with oxygen-15 and dynamic positron emission tomography. *J Cereb Blood Flow Metab* 6:105-119
- Johnson JA, Wilson TA (1966) A model for capillary exchange. *Am J Physiol* 210:1299-1303
- Kassissia IG, Goresky CA, Rose CP, Schwab AJ, Simard A, Huet P-M, Bach GG (1995) Tracer oxygen distribution is barrier-limited in the cerebral microcirculation. *Circ Res* 77:1201-1211
- Kety SS (1951) The theory and application of the exchange of inert gas at the lungs and tissues. *Pharmacol Rev* 3:1-41
- Kim S-G, Ackerman JH (1990) Quantification of regional blood flow by monitoring of exogenous tracer via nuclear magnetic resonance spectroscopy. *Magn Reson Med* 14:266-282
- Koeppel RA, Hutchins GD, Rothley JM, Hichwa RD (1987) Examination of assumptions for local cerebral blood flow studies in PET. *J Nucl Med* 28:1695-1703
- Larson KB, Markham J, Raichle ME (1987) Tracer-kinetic models for measuring cerebral blood flow using detected radiotracers. *J Cereb Blood Flow Metab* 7:443-463
- Lassen NA, Perl W (1979) *Tracer Kinetic Methods in Medical Physiology*, New York, Raven Press, p 168
- Ohta S, Meyer E, Fujita H, Reutens DC, Evan A, Gjedde A (1996) Cerebral ^{15}O water clearance in humans determined by PET: I. theory and normal values. *J Cereb Blood Flow Metab* 16:765-780
- Pekar J, Ligeti L, Ruttner Z, Lyon RC, Sinnwell TM, Van Gelderen P, Fiat D, Moonen CTW, McLaughlin AC (1991) *In vivo* measurement of cerebral oxygen consumption and blood flow using ^{17}O magnetic resonance imaging. *Magn Reson Med* 21:313-319
- Quarles RP, Mintun MA, Larson KB, Markham J, MacLeod AM, Raichle ME (1993) Measurement of regional cerebral blood flow with positron emission tomography: a comparison of ^{15}O water to ^{11}C butanol with distributed-parameter and compartmental models. *J Cereb Blood Flow Metab* 13:733-747
- Raichle ME, Martin WRW, Herscovitch P, Mintun MA, Markham J (1983) Brain blood flow measured with intravenous H_2^{15}O . II. Implementation and validation. *J Nucl Med* 24:790-798
- Renkin EM (1959) Transport of potassium-42 from blood to tissue in isolated mammalian skeletal muscles. *Am J Physiol* 197:1205-1210
- Sawada Y, Patlak CS, Blasberg RG (1989) Kinetic analysis of cerebrovascular transport based on indicator diffusion technique. *Am J Physiol* 256:H794-H812
- Takagi S, Kenny RJ, Gilson AJ (1984) A quantitative model for the measurement of cerebral vascular extraction fraction *in vivo* following intravenous injection: simulation studies. *J Cereb Blood Flow Metab* 4:564-573
- Williams DS, Detre JA, Leigh JS, Koretsky AP (1992) Magnetic resonance imaging of perfusion using spin inversion of arterial water. *Proc Natl Acad Sci USA* 89:212-216
- Zieler KL (1965) Equations for measuring blood flow by external monitoring of radioisotopes. *Circ Res* 16:309-321

An Adiabatic Approximation to the Tissue Homogeneity Model for Water Exchange in the Brain: II. Experimental Validation

Keith S. St. Lawrence and Ting-Yim Lee

Department of Diagnostic Radiology and the Lawson Research Institute, St. Joseph's Health Centre, and the Imaging Research Laboratories, Robarts Research Institute, London, Ontario, Canada

Summary: A frequently reported limitation to using water as a tracer for measuring CBF has been the dependence of the CBF estimate on the experimental time (referred to as the falling flow phenomenon, FFP). To eliminate the FFP, we have developed the adiabatic solution of the tissue homogeneity model to replace the solution of the single-compartment Kety model. In Part I, the derivation of the adiabatic solution was presented. In this second part, the adiabatic solution was applied to measure CBF in rabbits using nuclear magnetic resonance spectroscopy and the tracer deuterium oxide. It was shown that the FFP, observable when the ^2H clearance data

were analyzed with the Kety equation, was significantly reduced when the same data were analyzed with the adiabatic solution of the tissue homogeneity model. By concurrently measuring CBF with radioactive microspheres, it was determined that the CBF estimates from the adiabatic solution were accurate for true blood flow values less than $60 \text{ mL} \cdot 100 \text{ g}^{-1} \cdot \text{min}^{-1}$. Above this value the CBF estimate was progressively underestimated, which was attributed to the diffusion limitation of water in the brain. **Key Words:** Cerebral blood flow—Tracer kinetics—Deuterium oxide—Nuclear magnetic resonance spectroscopy.

In Part I, it was demonstrated that a time-domain, closed-form solution to the tissue homogeneity (TH) model (Johnson and Wilson, 1966; Sawada et al., 1989) can be derived using the adiabatic approximation. The motivation for this work was to develop a model that, on the one hand, is realistic enough to overcome the limitations of the Kety model in describing water transport in the brain (Kety, 1951), while, on the other hand, being simple enough to be useful in the analysis of data with limited temporal resolution.

The derived solution, or the adiabatic solution, was used to analyze ^2H -labeled water (D_2O) clearance data from the brain that was acquired using nuclear magnetic

resonance spectroscopy. This technique was chosen because it provided data with good signal-to-noise ratio. Since D_2O was injected into a peripheral vein and the arterial blood concentration of the tracer was determined throughout the experiment, the experimental procedure was analogous to that used in human studies with positron emission tomography (PET) (St. Lawrence et al., 1992). Additional steps were taken to ensure that other possible sources of the falling flow phenomenon (FFP) were accounted for in the experimental protocol. Such sources include timing errors in the input function (Iida et al., 1986; Koeppe et al., 1987), dispersion of the true input function (Iida et al., 1986), tissue heterogeneity (Gambhir et al., 1987), and arterial blood contamination (Koeppe et al., 1987; Ohta et al., 1996). Finally, the CBF estimates derived from the adiabatic solution were verified by concurrent measurements with radioactive microspheres (Heymann et al., 1977).

THEORY

The theoretical modeling that formed the basis for the data analysis in this study was outlined in Part I. The ^2H clearance data were analyzed with both the Kety equation (Equation 1 in Part I) and the adiabatic solution to the TH model (Equation 14 in Part I). As discussed in

Received February 24, 1997; final revision received January 6, 1998; accepted April 2, 1998.

This project was supported by the Medical Research Council of Canada, the National Cancer Institute of Canada, the Ontario Heart and Stroke Foundation, the Sterling-Winthrop Imaging Research Institute and the University Research Incentive Fund, Ontario Ministry of Colleges and Universities. Keith S. St. Lawrence was supported by a Medical Research Council of Canada Studentship and the Academic Development Fund of the London X-ray Associates.

Address correspondence and reprint requests to T.-Y. Lee, PhD, FCCPM, Department of Radiology, St. Joseph's Health Centre, 268 Grosvenor Street, London Ontario, Canada N6A 4V2.

Abbreviations used: CV, coefficient of variance; D_2O , ^2H -labeled water; FFP, falling flow phenomenon; FID, free-induction decay; PET, positron emission tomography; TH, tissue homogeneity.

Part I, for either solution CBF was determined from the exponential rate constant, which characterized the clearance of labeled water from brain tissue. For reference, the rate constant for the Kety equation is

$$k_{1c} = \frac{EF}{\lambda}, \quad (1)$$

where λ is the partition coefficient, E is the extraction fraction of water, and F is the blood flow of the tissue. For the adiabatic solution to the TH model, the rate constant is

$$k_{adb} = \frac{EF}{V_e} \quad (2)$$

where V_e is the volume of water in the extravascular space (EVS) of the tissue.

Effect of the arterial signal

The modeling process outlined in Part I only describes tracer transport in the microvasculature. Under experimental conditions, it is likely that larger vessels will contribute to the signal from the tissue (Feindel et al., 1965; Koeppe et al., 1987; Ohta et al., 1996). This additional vascular signal can be accounted for in the adiabatic solution (Equation 14 in Part I) by replacing the parameter V_i , which is the distribution volume of water in the microvasculature (IVS), with a larger vascular volume, V_b , that represents the volume of all blood-borne signal, including V_i

$$Q(t) = EF \int_0^t C_a(t-u) e^{-k_{adb}u} du + V_b C_a(t) \quad (3)$$

Effect of internal dispersion

It has been shown that the shape of the arterial blood curve measured at a peripheral artery can be distorted compared with the shape of the curve in the brain (Iida et al., 1986). This distortion is caused by the difference in the dispersion of the tracer as it passes from the heart to the brain compared with the dispersion from the heart to the peripheral arterial sampling site. Internal dispersion can be characterized by the following function (Iida et al., 1986)

$$d_i(t) = \frac{1}{\tau} \exp\left(\frac{-t}{\tau}\right) \quad (4)$$

where $d_i(t)$ is the internal dispersion function and τ is the internal dispersion time constant. The measured arterial blood curve, $C_{a,m}(t)$, at the peripheral site is related to the true arterial function, $C_a(t)$ by

$$C_{a,m}(t) = \frac{1}{\tau} \int_0^t C_a(t-u) \exp\left(\frac{-u}{\tau}\right) du \quad (5)$$

Using Equation 5, the Kety equation (Equation 1 in

Part I) can be expressed in terms of the measured arterial blood curve

$$Q(t) = F\tau C_{a,m}(t) + F(1 - \tau k) \int_0^t C_{a,m}(t) e^{-k_1 C(t-u)} du \quad (6)$$

Equation 6 has a form similar to the adiabatic solution (Equation 3). That is, the effects of internal dispersion and diffusion limitation of the tracer both lead to a fraction of the arterial blood curve being required in the solution for $Q(t)$. Therefore, the effect of internal dispersion must be determined separately if the diffusion limitation of water is to be investigated independently. A simple "bench top" experiment, which is outlined in the next section, was carried out to determine the effect of internal dispersion.

METHODS

Experimental procedure

Cerebral blood flow was measured in male New Zealand rabbits weighing 2.5 to 3.0 kg. Before an experiment, the rabbit was administered a preoperative dose of ketamine and xylazine (35 mg/kg ketamine mixed with 5 mg/kg xylazine) by intramuscular injection. An ear vein was catheterized and a tracheotomy performed while the rabbit was masked with 5% halothane. The rabbit was then ventilated with a mixture of O_2 and 1.5% isoflurane and paralyzed with an intravenous injection of pancuronium bromide (0.3 mg/kg), which was repeated at 1-hour intervals throughout the experiment. Catheters were inserted into a femoral vein, an ear vein, both femoral arteries, and the left atrium of the heart. To avoid signal contamination from scalp tissue, it was retracted to allow the surface coil to be placed directly on the skull.

After surgical preparation, the rabbit was wrapped in a recirculating water heating pad to maintain rectal temperature at 37°C. A three-turn surface coil with a diameter of 1.6 cm was placed on the rabbit's skull, and the rabbit together with the surface coil were positioned in the center of a horizontal bore Oxford magnet with a field strength of 1.89 T. Data acquisition was controlled by a Multi-Spec-IV2 console from Surrey Medical Imaging Systems (Surrey, U.K.). Arterial blood pressure was monitored throughout the experiment by means of a transducer connected to a femoral arterial catheter, and if required, phenylephrine (0.2 mg/mL) was infused into the ear vein to ensure that mean arterial blood pressure was maintained within the normal range (75 to 100 mm Hg). Before each CBF measurement, the blood gases were repeatedly measured to ensure they remained stable over a period of at least a half hour. Cerebral blood flow was measured twice in each animal, and the P_{aCO_2} was varied between trials (from 25 to 60 mm Hg) to obtain a range of CBF values. After each trial, the blood gases were again measured to determine whether the levels had remained constant during the experiment.

After the stabilization period, 10 mL of 99.1% D_2O with 0.9% NaCl was infused for 30 seconds into the femoral vein catheter. In none of the rabbits did the D_2O infusion cause any changes in the arterial blood pressure. An adiabatic radio frequency pulse, having its amplitude modulated by a hyperbolic secant function, was used for uniform excitation of the 2H nuclei in the brain (Baum et al., 1985). The repetition time between successive pulses was 750 ms, which was chosen to

allow the ^2H nuclei sufficient time to return to equilibrium before the next radio frequency pulse. The ^2H signal, which was the average of four free-induction decays (FID), was collected every 3 seconds. Owing to the rapid hydrogen-deuterium exchange, this signal reflected singly deuterated water HOD concentration in the brain (Ackerman et al., 1987). The ^2H data were collected for 1 to 2 minutes before injection (background signal) and for 15 minutes after injection. To determine the ^2H concentration in arterial blood during the experiment, arterial blood samples were collected at known time intervals throughout the experiment. The blood was withdrawn at a rate of 0.3 mL/min by a peristaltic pump connected to a femoral artery catheter. Using a fraction collector, the blood samples were collected over the following time intervals: 6 seconds for the first 3.5 minutes, 12 seconds for the next 3 minutes, and 30 seconds for the last 8.5 minutes. The concentration of HOD in each sample was determined after the experiment using the procedure described below.

Immediately after the completion of a D_2O washout experiment, CBF was measured using radioactive microspheres (Heymann et al., 1977). For the microspheres experiment, arterial blood was drawn from a femoral catheter at a rate of 1 mL/min for 3 minutes. At the 1-minute mark, 10 μCi of radioactive microspheres were injected into the left atrium. After the completion of both ^2H clearance trials and their respective microspheres experiments, the rabbit was killed and the brain removed. The brain was cut into small samples and each sample weighed. The content of radioactive microspheres in the tissue samples and the blood reference samples were assayed, and from this data, CBF was determined for each brain sample (Heymann et al., 1977).

The relative concentration of HOD in each of the blood samples collected during a D_2O washout experiment was determined using a small solenoid coil placed in the 1.89 T magnet (St. Lawrence et al., 1992). The number of FID collected for each sample depended on the time interval in which the sample was collected: 512, 200, and 64, respectively, for the time intervals listed previously. The measurement (see next paragraph) from each blood sample was scaled according to its weight and the number of FID averaged.

For both the tissue and the arterial blood data, processing consisted of multiplying each averaged FID with an exponential filter (4-Hz line-broadening factor), finding the complex frequency spectrum by fast Fourier transform, and calculating the magnitude of the complex frequency spectrum afterward. Each magnitude spectrum was then integrated with respect to frequency to determine the area under the ^2H peak. The individual peak areas were corrected for the background signal by subtracting the average peak area value determined from spectra collected before the injection of the D_2O . There were between 20 and 40 background spectra collected for the tissue data, and 5 for the arterial blood data.

Signal detection

As mentioned previously, the ^2H signal from the brain was detected using a surface coil. The finite extent and nonuniformity of the surface coil's field of reception of radio frequency waves necessitated the following modifications to Equation 3. To begin with, because the boundaries of the coil's sensitivity volume were not well defined, it was assumed that the coil detected signal originating from both gray and white matter in the brain (Ewing et al., 1989). To account for the signal from these two types of tissue, the adiabatic solution was summed over two rate constants in which the faster one represented blood flow in gray matter and the slower one represented blood flow in white matter (Obrist et al., 1967). In addition, the coil's

sensitivity to gray and white matter would be different depending on their respective locations relative to the coil. To account for these factors, Equation 3 was modified as

$$Q(t) = \sum_{j=1}^2 s_j w_j e \left(E_j F_j \int_0^t C_a(t-u) e^{-k_j u} du + (V_b)_j C_a(t) \right) \quad (7)$$

where the subscript j referred to either gray or white matter. All variables were defined previously, except w_j , which was the relative weight (fraction) of the j th type of tissue, and s_j , which represented the sensitivity of the coil to this tissue type. It was impossible to determine s_j without knowing the exact location of the j th tissue type relative to the coil. Consequently, although an individual CBF for each of the two tissue types could be determined from their respective rate constants, without knowing the s_j , the mean CBF for the specific mixture of gray and white matter in the sensitivity volume of the coil could not be determined.

Data analysis

In the curve-fitting analysis, all parameters before the integral sign for each tissue type in Equation 7 were lumped together as a single fitting parameter α_j , and the vascular volumes were combined as a single term $\alpha_b C_a(t)$. It is important to note that the fitting parameter, α_j , could not be used as a measure of the relative weight of the j th tissue since this parameter was also dependent on s_j . Because of the nonuniformity of the spatial sensitivity of the surface coil, s_j could not be determined, and therefore, its effect on the magnitude of α_j was unknown. A time shift (Δt) between the two data sets (the tissue and arterial blood concentration of HOD) was included in the fitting routine to account for the difference in time between the arrival of the tracer in the brain and the arrival of the tracer at the fraction collector (Meyer, 1989)

$$Q(t) = \sum_{j=1}^2 \alpha_j \int_0^t C_a(t - \Delta t - u) e^{-k_j u} du + \alpha_b C_a(t - \Delta t) \quad (8)$$

A constrained quasi-Newton algorithm was used in the regression analysis (Gill and Murray, 1974) to estimate the parameters in Equation 8. Besides the adiabatic solution of the TH model, the Kety equation was also used in the analysis. The Kety equation was also summed over two tissue types and its operational equation was given by Equation 8 without the $\alpha_b C_a(t)$ term. Note that in Equation 8 the subscript lc or adb on the rate constant was omitted. This omission was deliberate as the definition of a rate constant was not relevant to the regression analysis. When CBF was determined from the estimated rate constant, it was necessary to use either Equation 1 or 2, depending on the solution used in the analysis. For both solutions, the rate constants and scaling factors were constrained to have positive values since any negative values were nonphysiologic. A piecewise cubic Hermite interpolation routine was used to interpolate the arterial data to the same sampling interval as the tissue data (Gill and Murray, 1974).

To determine whether the estimates of the rate constants were independent of the experimental duration, the regression analysis was repeated using the Kety equation and the adiabatic solution with an increasing amount of data included with each successive repetition. The analysis began with the first 4 minutes of clearance data (the time of the initial rise of the ^2H clearance curve above background was taken as zero time), and with each repetition, an additional 1 minute of data was included in the analysis until the end of the clearance data set was reached (15 minutes). A starting duration of 4 minutes was

chosen because the clearance data did not reach its maximum value until roughly 2.5 minutes after injection because of the relatively long infusion duration (30 seconds) and the convolution of the data with the dispersion function of the sampling apparatus (see next section). For each increment, the percent difference of the higher rate constant (k_1) determined for the entire experimental duration from that determined for that time duration was calculated. The results were divided into two categories: (1) k_1 values corresponding to CBF measurements obtained using radioactive microspheres (CBF_M) that were less than $60 \text{ mL} \cdot 100 \text{ g}^{-1} \cdot \text{min}^{-1}$ (referred to as the flow-limited category), and (2) k_1 values corresponding to CBF_M values that were greater than $60 \text{ mL} \cdot 100 \text{ g}^{-1} \cdot \text{min}^{-1}$ (referred to as the diffusion-limited category). The value of $60 \text{ mL} \cdot 100 \text{ g}^{-1} \cdot \text{min}^{-1}$ was chosen as the boundary between these two categories because E was approximately 0.9 at this flow value (assuming $PS = 150 \text{ mL} \cdot 100 \text{ g}^{-1} \cdot \text{min}^{-1}$; Herscovitch and Raichle, 1987), and therefore, above this flow value, the effect of the diffusion limitation of water on the CBF estimate should become noticeable. With regard to the Kety equation, if the diffusion limitation of water were the primary factor contributing to the FFP, then the FFP should have been negligible for the flow-limited group since E was close to one. On the other hand, if there were a significant contribution from the larger vessels, then the FFP should have been observable at all flow values since this factor was independent of the diffusion limitations of the tracer (Koppe et al., 1987). For the adiabatic solution, the FFP should not be present in either category since the $\alpha_b C_a(t)$ term in Equation 8 had already accounted for all of the vascular signal. This analysis was not repeated for the lower rate constant (k_2) because of its significantly lower precision as compared with the precision of k_1 (see Fig. 6 in Part I).

External dispersion

A 1.0-m length of PE 60 surgical tubing (1.1 mL volume) was used to connect the fraction collector to the arterial catheter. This length of tubing was required to keep the sampling apparatus at a sufficient distance away from the magnet so as not to affect the detection of the ^2H signal. The presence of the tubing led to two artifacts in the measured arterial curve: a time delay with respect to the tissue data and a dispersion with respect to the true arterial curve. The time delay was accounted for in the regression analysis by the time shift variable discussed previously. The dispersion artifact was characterized by performing the following experiment.

The arterial blood sampling tubing, together with the arterial catheter and a three-way stopcock, was filled with saline. At time zero, one end of the tubing was dipped into a mixture of blood and D_2O . Using the peristaltic pump, samples were collected at 6-second intervals for 4 minutes after the submersion of one end of the tubing in the mixture, and the procedure was repeated four times. The HOD concentration in each sample was measured using the same procedure as with blood samples from the CBF experiments. The dispersion of a known input function can be expressed mathematically as (Iida et al., 1986)

$$C_m(t) = \int_0^t C_{true}(t-u) \text{disp}(u) du \quad (9)$$

where $C_{true}(t)$ is the known input function, $C_m(t)$ is the measured function, and $\text{disp}(t)$ is the dispersion function. In the dispersion experiments, the input function was a step function, which reduced Equation 9 to

$$C_m(t) = \int_0^t \text{disp}(u) du \quad (10)$$

The dispersion function, $\text{disp}(t)$, was assumed to be the sum of two gamma variate functions. The parameters of the gamma variate functions were determined by fitting Equation 10 to the measured curve, $C_m(t)$, using nonlinear regression techniques (Gill and Murray, 1974).

In principle, knowing the dispersion function of the sampling system, the true arterial blood curve could be determined by deconvolution. Instead, for the CBF experiments, the tissue data were convolved with $\text{disp}(t)$, which was equivalent to deconvolving the arterial data but easier to implement. If $Q_m(t)$ was the measured tissue curve, then the dispersed tissue curve, which was the data to be fitted by Equation 8 using nonlinear regression analysis, was given by

$$Q(t) = \int_0^t Q_m(u) \text{disp}(t-u) du \quad (11)$$

Internal dispersion

For these experiments, iodinated x-ray contrast agent (Isovue 300) was used as a tracer so that its concentration could be measured using the principle of absorptiometry (Yeung and Lee, 1992). The experimental setup consisted of a length of tubing with an internal diameter of 0.28 cm, a peristaltic pump, and the absorptiometry unit (Yeung and Lee, 1992). One end of the tubing was passed through the peristaltic pump before it was connected to the absorptiometry unit. The tubing had an additional 90-cm removable section that represents the distance from the left ventricle to the radial arteries in humans. This section was removed in baseline experiments and attached in the experiments designed to simulate dispersion in arteries. Before each experiment, the tubing was filled with water and, at time zero, the free end of the tubing was dipped into a reservoir of contrast solution (20 mg iodine/mL). The solution was pumped through the tubing at a rate (7 to 18 cm/s) controlled by the peristaltic pump, and the dispersion of the contrast agent was measured by the absorptiometry unit. Using the assumed internal dispersion function for arteries (Equation 4), the measured baseline dispersion curve was deconvolved with the measured arterial dispersion curve to determine the internal dispersion time constant τ .

RESULTS

Data analysis

A total of 44 trials (2 per rabbit) were attempted on 22 rabbits, with blood flows ranging from 30 to $150 \text{ mL} \cdot 100 \text{ g}^{-1} \cdot \text{min}^{-1}$. Six of the trials failed because of either technical errors or a change in PaCO_2 greater than 3 mm Hg in the rabbit during the experiment. The data obtained from one experiment are illustrated in Fig. 1. In the figure, time zero had been arbitrarily set to correspond to the time of the initial rise of the ^2H clearance curve above background, and the data before time zero represented the background values. The arterial data set had been shifted to the right to account for the time delay introduced by the arterial blood sampling apparatus. In the subsequent regression analysis, the relative positions of these two sets of data on the time axis were not important because a time shift (Δt) variable had been included as a fitting parameter. The data were presented in relative units only because no calibration between the blood and tissue data was performed owing to the nonuniform spa-

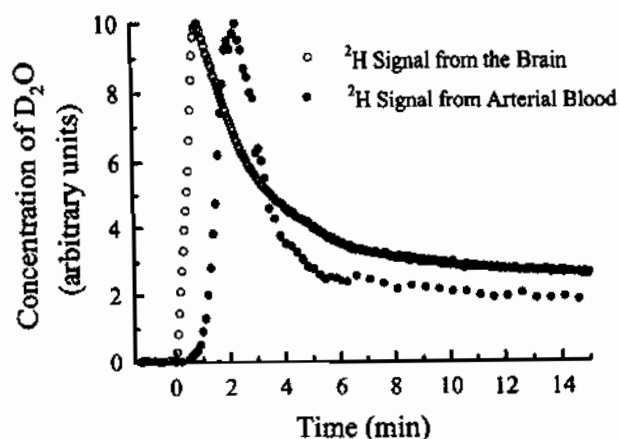


FIG. 1. The brain and arterial blood concentration of HOD as measured by nuclear magnetic resonance spectroscopy in a rabbit experiment. The brain and the arterial blood concentrations, both in arbitrary units, were plotted as functions of time. The time of the initial rise of the tissue data above background noise after the infusion of the D_2O was assumed to be time zero.

tial sensitivity of the surface coil. However, calibration was not necessary because CBF were determined from the rate constants only.

For both the Kety equation and the adiabatic solution, the time dependency of k_1 is illustrated in Fig. 2 for the 36 successful trials. The mean percent difference in k_1 as a function of experimental duration was plotted for the flow-limited group and the diffusion-limited group. From this graph it was apparent that the FFP was quite dramatic for both flow groups when the data were ana-

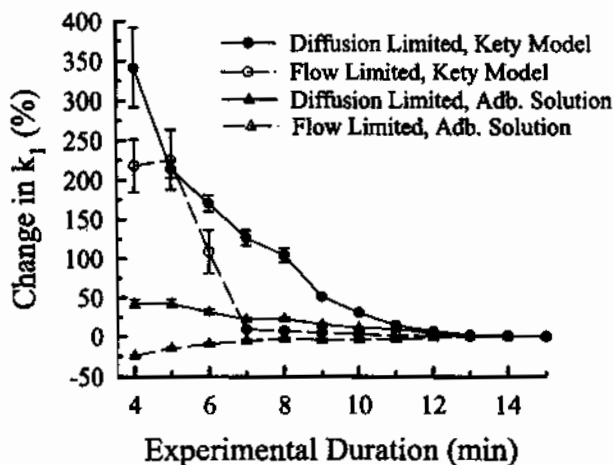


FIG. 2. The plot of percent difference of k_1 determined for the entire experimental duration from that determined for a particular experimental duration versus experimental duration. The data were divided into two groups: (1) CBF less than $60 \text{ mL} \cdot 100 \text{ g}^{-1} \cdot \text{min}^{-1}$ (flow-limited group), and (2) CBF greater than $60 \text{ mL} \cdot 100 \text{ g}^{-1} \cdot \text{min}^{-1}$ (diffusion-limited group). There were 12 trials in the flow-limited group and 24 trials in the diffusion-limited group. All data were analyzed using both the adiabatic solution of the tissue homogeneity model and the Kety equation. The data plotted were the mean percent differences of k_1 for each group, estimated using both solutions. The error bars were the standard errors of each group at the specific experimental duration. Adb., adiabatic.

lyzed using the Kety equation. In comparison, the FFP was reduced considerably when the data were analyzed using the adiabatic solution of the TH model.

For validation, the estimate of gray matter blood flow (CBF_g) from k_1 , as defined by Equation 2, was compared with the CBF_M for samples of tissue that were located just beneath the surface coil and were comprised mainly of cortical gray matter. Using a value of $94 \text{ mL} \cdot 100 \text{ g}^{-1}$ for V_e (Herscovitch and Raichle, 1985), CBF_g was calculated for all 36 trials using the higher rate constant estimated from the entire experimental duration. The CBF_g values are plotted in Fig. 3 as a function of the corresponding CBF_M measurements. The estimated value of the PS product for water was $140 \text{ mL} \cdot 100 \text{ g}^{-1} \cdot \text{min}^{-1}$, which was obtained by fitting Equation 4 from Part I to the data (Crone, 1963). This value was in good agreement with previously reported values for the PS product of the cerebral cortex (Herscovitch and Raichle, 1987).

Because of the mixing of gray and white matter in the other brain samples, an estimate of white matter blood flow was not obtained from the microspheres data. As a result, the CBF estimate from the lower rate constant, which represented white matter blood flow, could not be validated. Instead, the correlation between the k_2 estimates from the regression analysis and CBF_M is presented in Fig. 4. Although CBF_M represented gray matter blood flow, this graph did show the high degree of scatter in k_2 , which was caused by the low precision associated with this parameter. In Part I, we estimated that the coefficient of variation (CV) of k_2 was approximately 22%, which was considerably higher than the CV of k_1 ($\approx 7\%$). This reduction in precision can be attributed to the smaller weighting factor for this rate constant. Although the weighting factor for white matter is generally smaller

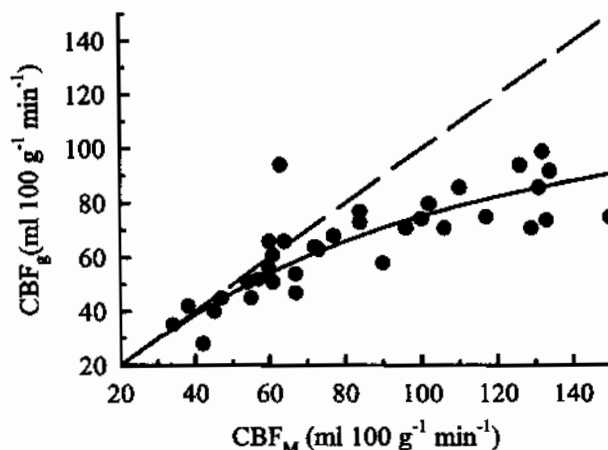


FIG. 3. The correlation between cortical gray matter CBF estimated by the adiabatic solution (CBF_g) and by radioactive microspheres (CBF_M). A total of 36 trials are presented and the dashed line is the line of identity. By fitting Equation 3 to the data, the PS product was estimated to be $140 \text{ mL} \cdot 100 \text{ g}^{-1} \cdot \text{min}^{-1}$.

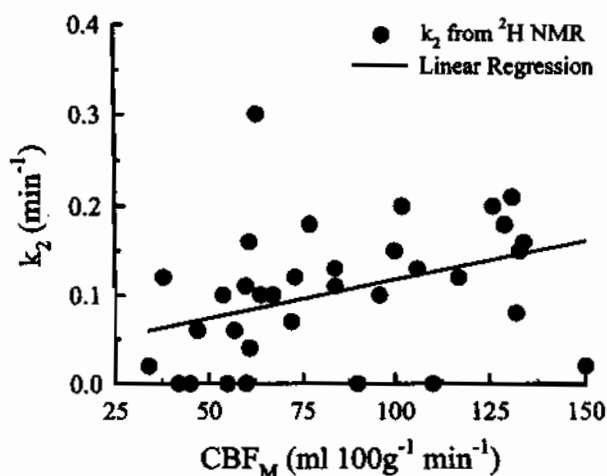


FIG. 4. The correlation between k_2 , as determined from the adiabatic solution, and CBF measured using radioactive microspheres (CBF_M). The results for the linear regression analysis were slope, 9×10^{-4} ; intercept, 0.03; and regression coefficient, 0.46; the relationship was statistically significant ($P < 0.05$).

than that of gray matter because of the lower blood flow in white matter, the value is further reduced by the surface coil's nonuniform sensitivity. The coil was most sensitive to the tissue immediately beneath it, which was cortical gray matter.

External dispersion

In Fig. 5, the averaged data set from the four trials of the external dispersion experiment is illustrated with the fit to the data using Equation 10 superimposed. The excellent agreement indicated that the dispersion caused by the blood sampling apparatus could be well represented by the sum of two gamma variate functions, which was the assumed external dispersion function. Figure 6 shows the convolution of the tissue curve from Fig. 1 with the external dispersion function in Fig. 5.

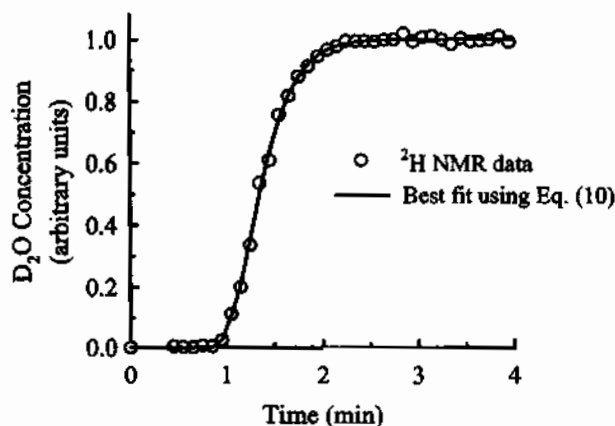


FIG. 5. The fit to the measured step-function response from the external dispersion experiments using Equation 10 is superimposed on the experimentally data. The external dispersion function used in the regression analysis was the sum of two gamma variate functions. The data shown were collected with a 6-second sampling interval and represent the average of four experiments.

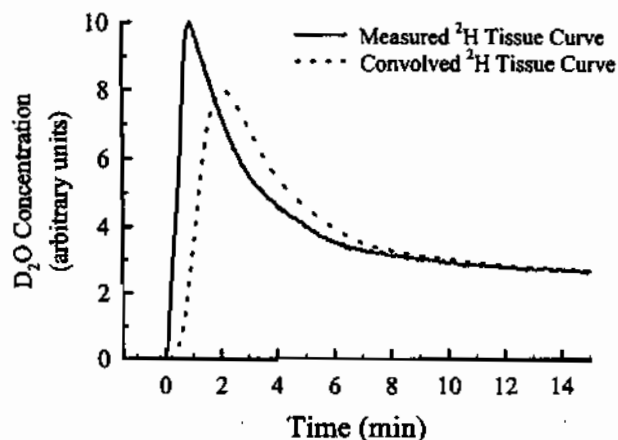


FIG. 6. The result of the convolution of the measured tissue clearance curve, which is displayed in Fig. 1, with the dispersion function of the blood sampling apparatus. It was the convolved data set that was fitted with Equation 8 to determine CBF.

The CV of the residuals of the averaged data set displayed in Fig. 5 from the fitted dispersion function was 1.3%. Using the covariance matrix method, which was outlined in Part I, we determined that the CV for any of the parameters defining the external dispersion function (see Equations 9–11) was less than or equal to 3%. By sequentially changing each parameter of the external dispersion function by two standard deviations, we determined that the largest expected error in the k_1 and k_2 estimates would be 3% and 7%, respectively. Therefore, any possible error in the characterization of the dispersion caused by the sampling apparatus would not significantly influence the CBF measurements.

Internal dispersion

The internal dispersion time constants measured for various flow velocities in the internal dispersion experiments are given in Table 1. For comparison, using color flow Doppler ultrasound the mean blood flow velocity in the radial artery of one volunteer was measured to be 18 cm/s. Because the path length difference found in the rabbit experiments was significantly shorter than 90 cm, the dispersion time constant must have been less than 0.4 seconds. Therefore, the influence of internal dispersion on the shape of the arterial curve would be negligible.

DISCUSSION

As demonstrated by the results in Fig. 2, the FFP was observable in both the flow-limited group and the diffu-

TABLE 1. Internal dispersion time constants measured for various flow velocities

Velocity (cm/s)	τ (s)
7	3.3
11	2.3
18	0.4

sion-limited group when the data were analyzed using the Kety equation. In the literature, various factors that may contribute to the FFP have been investigated. These factors included (1) tissue heterogeneity (Gambhir et al., 1987), (2) timing errors in the input function (Iida et al., 1986; Koeppe et al., 1987), (3) dispersion of the input function (Iida et al., 1986), (4) the inadequacy of the single-compartment model (Gambhir et al., 1987; Larson et al., 1987; Ohta et al., 1996), and (5) signal contamination from arterial blood (Koeppe et al., 1987; Ohta et al., 1996). Tissue heterogeneity could be disregarded as a possible explanation in this study because both the Kety equation and the adiabatic solution were summed over two tissue types. To avoid any error resulting from a time shift between the ^2H signal in tissue and in arterial blood, a time shift variable was included as a fitting parameter in the regression analysis (Meyer, 1989). Dispersion of the input function (arterial curve) could occur within both the subject (internal dispersion) or the sampling apparatus (external dispersion). The results in Table 1 demonstrated that the internal dispersion time constant was small for the flow velocities found in arteries, which were typically greater than 18 cm/s. Considering that the path difference within a rabbit was much shorter than the 90-cm length of tubing used in the experiments of Table 1, internal dispersion must have been insignificant in the rabbit experiments. External dispersion, although present, was explicitly accounted for by determination of the external dispersion function in separate dispersion experiments outlined previously. Therefore, in our CBF experiments neither source of dispersion could be considered the cause of the FFP.

We believe that the FFP arises from the remaining two factors: inadequacy of the Kety model in describing water transport in the brain and signal contamination from arterial blood. It has been demonstrated theoretically that water transport in the brain would be better described by a two-compartment model (Gambhir et al., 1987). Our data support this hypothesis and complement the findings of Ohta et al. (1996), who investigated the effect of a vascular contribution on CBF measurement using PET and the tracer H_2^{15}O . As the results in Fig. 2 illustrated, when the Kety model was used to analyze data from the diffusion-limited group, there was a consistent decrease in the k_1 estimate as the experimental duration increased. By using the adiabatic solution instead of the Kety equation, the trend was significantly reduced, although not entirely eliminated. Even with the adiabatic solution, the mean k_1 for the 4 minutes of experimental time was 40% greater than k_1 for the entire experimental duration, which was attributed to the correlation between the fitting parameters α_b and k_1 (see Table 3, Part I). As discussed in the previous article, the correlation between these two parameters could be eliminated by increasing the experimental duration to more than 9 minutes. There

was also a bias introduced into the k_1 estimate derived from the analysis with the Kety equation, which was the result of the constraints imposed in the regression analysis. However this bias was not large enough to explain the FFP associated with this model. Therefore, the observed FFP must be a result of the inadequacy of the Kety model in accounting for the diffusion limitation of labeled water.

If the FFP were only a result of the diffusion limitation of the tracer in the microvasculature, then it should not have been observed for the flow-limited group when the data were analyzed with the Kety equation. However, the results illustrated in Fig. 2 showed a large overestimation of k_1 for early integration times, although for times greater than 6.5 minutes the k_1 estimate was stable. We believe that this overestimation of k_1 was a result of the blood-borne signal arising from outside the capillary space, such as from a major artery. The significance of the arterial blood volume has been recently demonstrated by Ohta et al. (1996). Using PET they were able to generate maps of the vascular volume, and from these maps it was clearly demonstrated that the vascular volume increased dramatically near major arteries. With the adiabatic solution, the arterial blood-borne signal was accounted for by the term $\alpha_b C_a(t)$, and as a result, the estimate of k_1 was relatively stable over all integration times for the flow-limited group.

Even though the adiabatic solution significantly reduced the FFP, the results in Fig. 3 demonstrated that this solution was only able to accurately measure CBF at flow rates less than $60 \text{ mL} \cdot 100 \text{ g}^{-1} \cdot \text{min}^{-1}$. Above this threshold, the CBF estimate was appreciably underestimated because of the limited extraction of water into the parenchymal tissue. These results were similar to what had been previously reported for CBF measurements using the tracer H_2^{15}O (Raichle et al., 1983). It had been demonstrated that if CBF was to be measured accurately at all values, then compartmental models had to be abandoned in favor of the more physiologically realistic distributed-parameter models (Goresky et al., 1976; Rose et al., 1977; Larson et al., 1987). Unfortunately, as discussed in Part I, the solutions to distributed-parameter models were considerably more complex than the adiabatic solution. Furthermore, there were other experimental limitations that had to be considered, such as (1) the arterial blood-borne signal, and (2) tissue heterogeneity. Regardless of the model chosen, these factors will influence the CBF estimate if they are not accounted for in the modeling. A distributed-parameter model had been used to analyze data acquired with PET, and it was concluded that owing to the noise limitations of PET images, implementing such a model was unrealistic (Quarles et al., 1993). For our study the adiabatic solution represented a reasonable compromise between experimental reality and the true complexity of water transport in the brain.

In summary, experimental data were presented that verified the ability of the adiabatic solution of the TH model to properly describe the transport of water in the brain. From the data analysis, it was determined that the adiabatic solution was capable of significantly reducing the FFP that was observed when clearance data were analyzed with the Kety equation. By accounting for other possible sources of the FFP, we believe this phenomenon can be attributed to the diffusion limitation of water and the arterial blood-borne signal. For validation of the adiabatic solution, CBF was concurrently measured with radioactive microspheres. By comparing the microspheres CBF estimates with the estimates from the adiabatic solution, it was also demonstrated that the latter could accurately measure CBF for flow values less than 60 mL·100 g⁻¹·min⁻¹. Above this value, the diffusion limitation of water resulted in a progressive underestimation of CBF by the adiabatic solution as the true value of CBF increased.

Acknowledgments: The authors thank Monique Labodi and Jane Sykes for their technical assistance. The authors also thank Sarah Henderson and Dr. Ivan Yeung for their many valuable suggestions.

REFERENCES

- Ackerman JH, Ewy CS, Becker NN, Shalwitz RA (1987) Deuterium nuclear magnetic resonance measurements of blood flow and tissue perfusion employing ²H₂O as a freely diffusible tracer. *Proc Natl Acad Sci USA* 84:4099-4102
- Baum J, Tycho R, Pines A (1985) Broadband and adiabatic inversion of a two-level system by phase-modulated pulses. *Phys Rev* 32: 3435-3447
- Crone C (1963) The permeability of capillaries in various organs as determined by use of the 'indicator diffusion' method. *Acta Physiol Scand* 58:292-305
- Ewing JR, Branch CA, Helpert JA, Smith MB, Butt SM, Welch KMA (1989) Cerebral blood flow measured by NMR indicator dilution in cats. *Stroke* 20:259-267
- Feindel W, Garretson H, Yamamoto L, Perot P, Rumin N (1965) Blood flow patterns in the cerebral vessels and cortex in man studied by intracarotid injection of radioisotopes and coomassie blue dye. *J Neurosurg* 23:12-22
- Gambhir SS, Huang S-C, Hawkins RA, Phelps ME (1987) A study of the single compartment tracer kinetic model for the measurement of local cerebral blood flow using ¹⁵O-water and positron emission tomography. *J Cereb Blood Flow Metab* 7:13-20
- Gill PE, Murray W (1974) *Numerical Methods for Constrained Optimization*, London, Academic Press
- Goresky CA, Ziegler WH, Bach GG (1976) Capillary exchange modelling: barrier-limited and flow limited distribution. *Circ Res* 27: 739-764
- Herscovitch P, Raichle ME (1985) What is the correct value for the brain-blood partition coefficient for water? *J Cereb Blood Flow Metab* 5:65-69
- Herscovitch P, Raichle ME (1987) Positron emission tomographic measurement of cerebral blood flow and permeability-surface area product of water using [¹⁵O]water and [¹¹C]butanol. *J Cereb Blood Flow Metab* 7:527-542
- Heymann MA, Payne BD, Hoffman JIE, Rudolph AM (1977) Blood flow measurements with radionuclide-labelled particles. *Prog Cardiovasc Dis* 10:55-79
- Iida H, Kanno I, Miura S, Murakami M, Takahashi K, Uemura K (1986) Error analysis of a quantitative cerebral blood flow measurement using H₂¹⁵O autoradiography and positron emission tomography, with respect to the dispersion of the input function. *J Cereb Blood Flow Metab* 6:536-545
- Johnson JA, Wilson TA (1966) A model for capillary exchange. *Am J Physiol* 210:1299-1303
- Kety SS (1951) The theory and application of the exchange of inert gas at the lungs and tissues. *Pharmacol Rev* 3:1-41
- Koeppel RA, Hutchins GD, Rothley JM, Hichwa RD (1987) Examination of assumptions for local cerebral blood flow studies in PET. *J Nucl Med* 28:1695-1703
- Larson KB, Markham J, Raichle ME (1987) Tracer-kinetic models for measuring cerebral blood flow using detected radiotracers. *J Cereb Blood Flow Metab* 7:443-463
- Meyer E (1989) Simultaneous correction for tracer arrival delay and dispersion in CBF measurements by the H₂¹⁵O autoradiographic method and dynamic PET. *J Nucl Med* 30:1069-1078
- Obrist DO, Thompson HK, King CH, Wang HS (1967) Determination of regional cerebral blood flow by inhalation of 133-xenon. *Circ Res* 20:124-135
- Ohta S, Meyer E, Fujita H, Reutens DC, Evan A, Gjedde A (1996) Cerebral [¹⁵O]water clearance in humans determined by PET: I. theory and normal values. *J Cereb Blood Flow Metab* 16:765-780
- Quarles RP, Mintun MA, Larson KB, Markham J, MacLeod AM, Raichle ME (1993) Measurement of regional cerebral blood flow with positron emission tomography: a comparison of [¹⁵O]water to [¹¹C]butanol with distributed-parameter and compartmental models. *J Cereb Blood Flow Metab* 13:733-747
- Raichle ME, Martin WRW, Herscovitch P, Mintun MA, Markham J (1983) Brain blood flow measured with intravenous H₂¹⁵O. II. Implementation and validation. *J Nucl Med* 24:790-798
- Rose CP, Goresky CA, Bach GG (1977) The capillary and sacrolemmal barriers in the heart. *Circ Res* 41:515-533
- Sawada Y, Patlak CS, Blasberg RG (1989) Kinetic analysis of cerebrovascular transport based on indicator diffusion technique. *Am J Physiol* 256:H794-H812
- St. Lawrence KS, Lee T-Y, Yeung WTI (1992) Cerebral blood flow measurement with deuterium oxide: determination of the arterial concentration of the injected tracer. *11th Meeting of the Society of Magnetic Resonance in Medicine*, p 1108
- Yeung IWT, Lee TY (1992) An absorptiometry method for the determination of arterial blood concentration of injected iodinated contrast agent. *Phys Med Biol* 37:1741-1758